Tuning features of H-bonded layer by layer assembly of poly(4-vinyl pyridine) and carboxylated poly-(2,3,4,5,6-pentafluorostyrene) synthesized through para-fluoro-thiol reaction

Quanyi Yin, Emmanuel Beyou, Daniel Portinha, Aurélia Charlot

Tuning features of H-bonded Layer by Layer assembly of poly(4-vinyl pyridine) and carboxylated poly-(2,3,4,5,6-pentafluorostyrene) synthesized through para-fluoro-thiol reaction

Quanyi Yin [a,b], Emmanuel Beyou [b], Daniel Portinha [a*], Aurélia Charlot [a*]

[a] Université de Lyon, INSA-Lyon, UMR CNRS 5223, Ingénierie des Matériaux Polymères, F-69622 Villeurbanne Cedex, France

[b] Université de Lyon, Université Lyon 1, UMR CNRS 5223, Ingénierie des Matériaux Polymères, F-69622 Villeurbanne Cedex, France

Corresponding authors: Tel.: +33 4 72 43 63 38; fax: +33 4 72 43 85 27.

E-mail addresses: daniel.portinha@insa-lyon.fr, aurelia.charlot@insa-lyon.fr

ABSTRACT

Para-fluoro-thiol reaction (PFTR) was applied to poly(2,3,4,5,6-pentafluorostyrene) (PPFS) with mercaptopropionic acid (MPA), resulting in a library of carboxylated-PPFS copolymers (PPFS-MPA) differing in their chemical composition. The ability of these COOH-containing derivatives to develop H-bonds with poly(4-vinyl pyridine) (P4VP) in solvent solution was investigated, and it was shown that the extent of the H-bonded complexes was closely influenced by the degree of PPFS modification and by the nature of solvent. Subsequently, the Layer by Layer stepwise deposition of P4VP and PPFS-MPA was achieved from various deposition solvents. It was demonstrated that the use of DMF as solvent does not allow for the formation of LbL films, due to its competitive H-bond acceptor character. In contrary, when solvents such as $CHCl_3$ and MEK are respectively utilized for P4VP and PPFS-MPA, thick (P4VP/PPFS-MPA)-based LbL films constituted of interpenetrated layers are obtained and the topography is smooth and rather featureless. The use of ethanol as deposition solvent for both P4VP and PPFS-MPA leads to very thin films made of well-stratified polymer layers, with a nodular and patchy surface morphology.

Keywords

PPFS - para-fluoro-thiol reaction - carboxylic acid groups - interpolymer complexes - H-bonds - multilayer films - LbL assembly

1. Introduction

In the polymer nanomaterial science area, a great attention has been dedicated to thin polymer films. Such films and their formation are very relevant from fundamental aspect together with a high potential to bring specific functionalities to a given substrate. Among the various strategies to generate polymer films, the Layer by Layer (LbL) self-assembly has emerged as a key bottom-up approach to engineer so-called multilayer films [1,2]. This approach is very attractive in terms of simplicity, robustness and versatility as well as tailored properties of the films that may result (precise control of the thickness, the architecture, the composition at the nanoscale) [3-5]. Interestingly, LbL assembled films find versatile applications in specific technological fields [6-9]. Most of LbL assemblies originate from the development of supramolecular interactions. Even if a large panel of non-covalent interactions was exploited to design LbL films [10-13], electrostatic interactions [14-17] and H-bonds represent the most conventional exploited forces to build-up nanolayered films [18-20]. H-bonds are particularly interesting, since they offer a high level of versatility and are sensitive to various environmental stimuli [19]. Polymers able to develop H-bonds include polyesters, polyacrylates, pyridine derivatives, polyethers [21], polyamides [22] or natural polymers, such as polysaccharides [23] or lignin [24]. For example, Stockton and Rubner described H-bonds driven LbL assembly of polyaniline (as H-bond donor) with different non-ionic H-bond acceptor polymers, such as poly(vinylpyrrolidone) (PVPON), poly(vinyl alcohol) (PVA), poly(acrylamide) (PAAM), and poly(ethylene oxide) (PEO) [25]. The most prominent examples deal with the use of COOH-containing polymers as H-bond donors [19], deposited from aqueous medium and poly(acrylic acid) (PAA) [26,27] and poly(methacrylic acid) (PMAA) [28] are the most popular building blocks in H-bonded LbL assemblies area. For instance, Lee *et al*. [29] reported multilayer films of PVA and weak polyacids (PAA or PMAA) deposited from aqueous acidic solutions. Li *et al*. [30] prepared antifouling and self-

healing polymeric LbL films composed of partially hydrolyzed poly(2-ethyl-2-oxazoline) (PEtOX) and PAA. Conductive films were designed by Delongchamp *et al*., who used PEO and PAA [31] and by Cui *et al*. [32], who prepared original H-bonded films from the deposition of aqueous solutions of PEG-α-cyclodextrin complexes and PAA. (PEO/PAA) and (PEO/PMMA) films were also in-depth investigated by Sung *et al*., who established a link between the thickness and the glass temperature of the film [33]. LbL films were also obtained through the assembly of a lignin derivative containing carboxylic acid groups and poly(4-vinyl pyridine) (P4VP) [24], able to develop both H-bonds and electrostatic interactions. Zhang *et al*. [34] prepared multilayers of carboxylated-dendrimers with P4VP through LbL assembly of alcoholic solutions. They obtained porous films after extraction of dendrimers by a basic solution. The same research team also prepared microporous (PAA/P4VP) films [35]. More recenty, films based on poly(N-vinylamide) derivatives and tannic acid were assembled from acetonitrile solutions [22]. However, only a few groups have studied the influence of the nature of the deposition solvent onto the LbL assembly. Zhunuspayev *et al.* [36] elaborated films based on PAA and PVPON, by using various solvents (water at different pH, and a series of alcohols). They showed that the solvent allowing for the strongest complexation also led to the thickest LbL film. Ma *et al* [37] studied the effect of solvent (water, alcohol, DMSO, dimethylacetamide, tetramethylurea and N-methyl pyrrolidone) on the formation of the H-bonded (PAA/PVPON) film. They demonstrated that LbL films could be assembled when interactions between the interacting polymer and the solvent are not predominant and they showed that the chain conformation impacts the assembly process. Chen *et al.* investigated polyacrylate-containing films constructed from various solvent mixtures and they established a link between the size of polymer coil in solution and the LbL assembling process [38].

In summary, despite the plethora of articles dealing with the design of H-bonded LbL films,

which cannot be exhaustively itemized herein, such multilayered films are still challenging. In order to enlarge this research area, the synthesis of tailor-made H-bond donor (co)polymers allows for engineering novel categories of H-bonded films achievable in not so-common solvents. In this frame, we have recently prepared new H-bonded LbL assembly from the deposition of hydroxylated poly(2,3,4,5,6 pentafluorostyrene) (PPFS) derivatives and P4VP, as a strong H-bond acceptor [39]. These OH-containing polymers were synthesized by the para-fluoro-thiol reaction (PFTR) [40-43]. Indeed, our group is actively involved in PPFS modification through PFTR that allows for modifying the *para* position of the fluorinated ring by heterofunctional mercapto-derivatives in presence of a base [44, 45]. Thus, we prepared a library of hydroxylated PPFS copolymers, on which polyfluorinated or hydrogenated hydroxyl groups were attached and we showed that the OH chemical environment controls the growth process, the internal organization and the morphology of the LbL films [39].

Herein, we focus on the attributes of COOH groups and we report the synthesis of carboxylated-PPFS derivatives by PFTR with mercaptopropionic acid (MPA), as thiol modifier. The experimental parameters were tuned in order to generate a panel of PPFS-MPA copolymers differing in the extent of modification. The ability of the PPFS-MPA derivatives to develop H-bonds with P4VP in solution was investigated and the interacting properties between these two partners were advantageously exploited to engineer H-bonded LbL assembly. In particular, we focused on the influence of the extent of PPFS modification, and especially on the nature of the solvent deposition (separated solvents $CHCl_3$ for P4VP and MEK for PPFS-MPA, DMF, and EtOH) onto the growth mechanism, the thickness, the topography of the LbL films and the internal structure of the layered interacting chains. Such study is the cornerstone for further applicative exploitation in the field of thin polymer films engineering.

2. Experimental section

2.1 Materials

Chloroform ($CHCl_3$, 99%), methyl ethyl ketone (MEK, 99%), ethanol (EtOH, 99%) N, N-dimethylformamide (DMF, 99%), 1,8-diazabicyclo[5.4.0]undec-7-ene (DBU, 98%), mercaptopropionic acid (MPA, 99%) and poly(4-vinylpyridine) (P4VP, 60000 g/mol) were purchased from Sigma Aldrich and used as received. Quartz and silicon slides were purchased from Carl-Roth and SIL'TRONIX, respectively. Poly(2,3,4,5,6-pentaflurostyrene) (PPFS, 14000 g/moL, Đ = 1.2) was synthesized and characterized as described elsewhere [43].

2.2 Characterization methods

2.2.1 Nuclear magnetic resonance spectroscopy (NMR).

^{1}H and ^{19}F-NMR spectra for polymeric samples were recorded on a Bruker Advanced AM400 spectrometer at 400 MHz. The experiments were performed at room temperature using 5mg of polymer diluted in 1 mL of DMF-d_7. Chemical shifts were determined in ppm. ^{1}H-NMR spectra were calibrated thanks to tetramethylsilane at 0 ppm, while ^{19}F-NMR spectra were calibrated thanks to the signal at -143 ppm that corresponds to the fluorine in (ortho + ortho') positions (**Fig. S1**).

2.2.2 Attenuated total reflection fourier transform infrared (ATR FT-IR).

ATR FT-IR spectra were collected using a Nicolet iS10 apparatus (diamond crystal) with a resolution of 4 cm^{-1} in the 500-4000 cm^{-1} range.

2.2.3 Wettability properties measurements.

Water contact angles (θ_{water}) and water hysteresis measurements ($\Delta\theta_{water}$) were performed on a Dataphysics Digidrop contact angle meter equipped with a CDD2/3 camera. A droplet of 5 µL milli-Q-quality water was produced by a micro syringe and five measurements at different locations of each sample were done to get an average with a standard deviation. The contact angle hysteresis is the difference between the advancing water contact angle ($\theta_{a)}$ and

the receding water contact angle (θ_r). Advancing contact angle measurements were obtained by feeding water droplets and receding contact angle measurements were measured by removing water from the droplets. θ_a corresponds to the angle of a water droplet deposited onto a not previously wetted surface, and the θ_r angle corresponds to the angle of a water droplet deposited onto a surface that was previously wetted. The water hysteresis reflects the presence of surface heterogeneities: chemical or/and topographic ones.

2.2.4 Ultraviolet spectroscopy (UV).

UV spectra of the films assembled on quartz slides (1.5 cm × 3.5 cm) were directly recorded on a Shimadzu UV-2550 spectrophotometer in transmission mode.

2.2.5 X-ray photoelectron spectroscopy (XPS).

XPS analysis of the surfaces was conducted on a PHI Quantera SXM Spectrometer using an aluminium Kα X-ray radiation source with a photon energy of 1486.6 eV. The pressure in the chamber was below 10^{-9}-10^{-10} torr before data were taken, and the voltage and current of the anode were set at 15 kV and 3 mA, respectively. The pass energy was 40 eV. The binding energy scale was fixed with setting the C1s peak maximum at 285.0 eV.

2.2.6 Atomic force microscopy (AFM).

AFM images were acquired in intermittent contact mode (tapping mode), on silicon wafer with a size of 1 cm × 1 cm, in air at room temperature using an AFM Bruker Multimode 8 apparatus equipped with Nanoscope V controller. The scanning speed for image acquisition is 0.5 Hz. The used tips were purchased from Bruker with the model of SCANASYST-AIR. The surface root mean square roughness (Rq) was obtained by processing images using the Nanoscope Analysis software (version 1.5). In order to access the film thickness, an indentation was delicately performed with a razor blade by ensuring a good access to the silicon substrate and the elimination of the removed polymer from the surface. The height difference created by the indentation can be probed by AFM topology, which provides the

film thickness. Five measurements were made on each sample to obtain an average dry film thickness.

2.3 Modification of PPFS by PFTR

PPFS was modified by Mercaptopropionic acid (MPA) in the presence of DBU as base *via* para-fluoro-thiol-reaction. In a typical procedure, PPFS (0.5 g, 2.6 mmoL PFS units) was dissolved in 2.8 mL of MEK followed by the addition of MPA (2.6 mmoL, 2.30 mL) and DBU (1.82 mmoL, 0.27 mL) in MEK such that (PFS):(-SH):(DBU) molar ratio is 1:1:0.7. The mixture was stirred for 6 h at room temperature. After dilution with DMF, the resulting polymers were isolated by precipitation into cold acidic water (pH < 3) and washed with water until no residual thiol or base was revealed by ^{1}H-NMR. The collected polymers were dried at 40 °C under vacuum for 12 hours with a yield of 81%. A degree of substitution (DS) of 32% was determined by ^{19}F-NMR, through the calculation of the integral area ratio of the meta'-fluorine atoms of modified PFS units located at δ = −133 ppm to the ones located at δ = −143 ppm (ortho'- and ortho-fluorines of overall PFS units) (see **Figure S1**). Specimens are then designated as PPFS-MPA with their respective DS in the text (PPFS-MPA-DS).

2.4 Preparation of P4VP/PPFS-MPA blends.

Blends were obtained by simply mixing appropriate amounts of PPFS-MPA with P4VP that were separately dissolved in a given solvent. Typically, 30 mg of PPFS-MPA-32% copolymer was dissolved in 5 mL of $CHCl_3$/MEK (v/v = 1/1), EtOH or DMF. Then, an appropriate amount of H-bonds acceptor P4VP was separately dissolved in the same volume of solvent ($CHCl_3$/MEK, EtOH or DMF) and then added in the PPFS-MPA solution in order to obtain a -COOH:4VP ratio of 1:6. The mixtures were stirred for 10 min and pictures were taken. After a slow evaporation of the solvent ($CHCl_3$/MEK and EtOH) in glass vials at room temperature, the resulting solid samples were dried at 25 °C under vacuum for two days. For the samples

prepared in DMF, solvent was slowly evaporated at 50 °C and dried at 70 °C under vacuum for two days. The obtained solid polymer mixtures were analyzed by FT-IR in ATR mode and XPS.

2.5 Preparation of H-bonded multilayer films

Silicon or quartz slides were cleaned by 15 min intervals of sonication in acetone, ethanol, and Milli-Q water. After dried under gentle nitrogen flow, they were activated by ozonolysis for 30 min and then readily used. In a typical procedure, LbL assembly was started by immersing the freshly activated substrate into a P4VP solution (2 g/L) in EtOH for 5 min, followed by rinsing with the same solvent for 1 min statically. After drying with gentle nitrogen flow, the substrate was transferred into the PPFS-MPA-32% solution (2 g/L) in EtOH for 5 min and then rinsed with the corresponding solvent using the same procedure than the one used for P4VP layer, followed by drying process with a nitrogen flow. The combination of these two steps corresponds to the formation of a so-called one bilayer (BL). The procedure was repeated n times to deposit n BL and with using other solvents such as DMF for both P4VP and PPFS-MPA and $CHCl_3$ for P4VP combined to MEK for PPFS-MPA. The deposition process was monitored by FT-IR in ATR mode or/and by UV spectroscopy, the driving force was characterized by ATR FT-IR and XPS and the surface features were evaluated by water contact angle measurements and by AFM imaging.

3. Results and discussion

3.1. Synthesis of the carboxylated-PPFS derivatives

In order to synthesize carboxylic acid-containing PPFS based polymers, para-fluoro-thiol reaction (PFTR) was applied to poly(2,3,4,5,6-pentaflurostyrene) (PPFS) in presence of mercaptopropionic acid (MPA) as a functional thiol (**Scheme 1**). In such reaction, a non-nucleophilic base is used as co-reactant to prepare *in-situ* a thiolate specie that is active toward PPFS. Valtola *et al.* [46] used triethylamine for the modification of PS-b-PPFS with thioglycolic acid at room temperature in DMF and they obtained a degree of substitution (DS) of 14% after 4h. Noy *et al.* [47] recently demonstrated that 1,8-diazabicycloundec-7-ene (DBU) was a very efficient base for PFTR whatever the chemical structure of the thiol is. Indeed, quantitative PFTR was obtained after 3 to 80 min at 25-45 °C, depending on the employed thiol.[47] This procedure was also applied to COOH-containing thiol such as MPA or amino acid L-cysteine for the modification of (pentafluorophenyl)ester amide-containing poly(methacrylates). Considering the afore-mentioned results, we selected DBU as the co-reactant and the PFTR was conducted at room temperature in MEK, a non-protic polar solvent that is known to favor the substitution reaction [40].

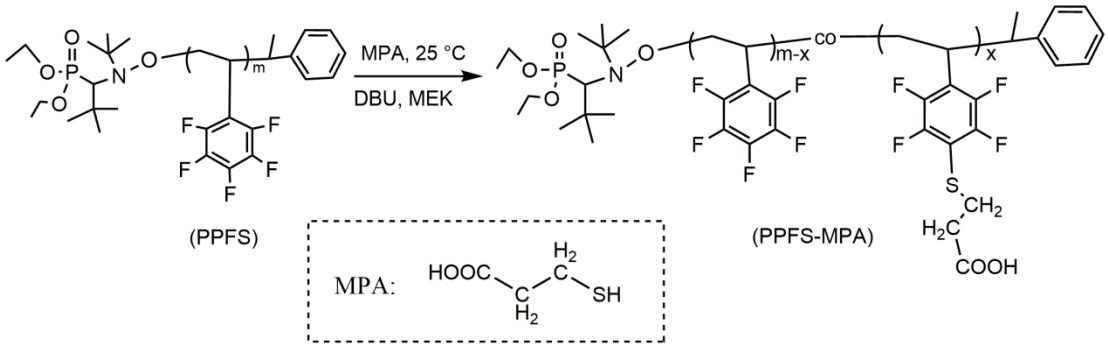

Scheme 1. Modification of PPFS by para-fluoro-thiol reaction with mercaptopropionic acid.

Before discussing the influence of the [PFS units]:[Thiol]:[DBU] concentration ratio on the extent of PPFS modification, namely the DS of the polymer, the expected substitution reaction was firstly qualitatively evidenced by FTIR analysis after the purification step (see experimental part). Figure 1 corresponds to the ATR FT-IR spectra of the sample obtained after a reaction time of 360 minutes. The latter polymer is referred as PPFS-MPA-32%, corresponding to a DS value of 32 %, as determined by ^{19}F NMR (**Fig. S1**).

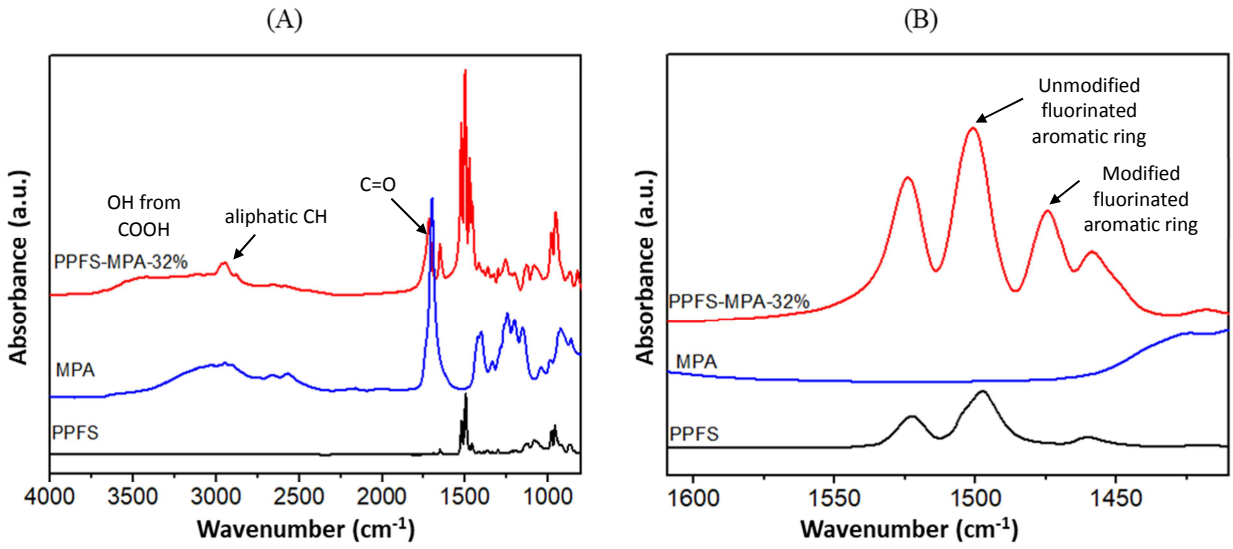

Fig. 1. ATR FT-IR spectra of (A) PPFS, MPA and PPFS-MPA-32% and (B) enlarged spectra in the range of 1400-1600 cm^{-1} (For experimental conditions, see Table 1, entry 3).

From Fig. 1 (A), as compared to MPA and pristine PPFS, it can be observed that new peaks appear for the PPFS-MPA-32% sample at 1720 cm^{-1} and in the 2250-3750 cm^{-1} range which can be respectively ascribed to the C=O and O-H stretching vibrations of the COOH groups. Moreover, as shown in Fig. 1 (B), the fluorinated aromatic ring vibrations of unmodified PFS units are located around 1500 cm^{-1}, while the vibrations of the PFS units modified in *para*-position appear around 1480 cm^{-1} [41]. ^{19}F-NMR spectroscopy confirms the regioselectivity of the PFTR (**Fig. S1**). Indeed, pristine PFS units exhibit three distinct characteristic signals at

-143 ppm, -154 ppm and -161 ppm, assigned to the fluorine atoms in *ortho*, *para* and *meta* positions, respectively. Upon modification, a new peak that is downfield shifted around - 135 ppm appears that is associated to the fluorine atoms located in *meta* position (named "*meta*'), while the signal of the fluorine atoms located in *ortho* position (named "*ortho*') cannot be distinguished from the one of the fluorine atoms in *ortho* position of unmodified units [48]. Herein, a small upfield shift of the signal of the fluorine atoms of remaining unmodified units (to -157 ppm and -164 ppm) is also observed, attesting that their chemical environment is somehow affected by the close presence of COOH polar groups. The DS can be easily calculated by comparing the values of the integral area ratio determined in the ^{19}F NMR spectra (see experimental section). Both spectroscopic techniques confirm the chemo- and regioselectivity of the PFTR conducted with MPA as a modifier. Several experiments were achieved by varying the [PFS units]:[MPA]:[DBU] concentration ratio, either by increasing the DBU content for a constant [PFS units]:[MPA] ratio, or by increasing the [MPA] content (**Table 1**). Indeed, these two routes allow for tuning the DS [42, 43]. Herein, it was observed that for a [PFS units]:[MPA]:[DBU] of 1:1:0.4, no PFTR occurs even after 4 hours (**Table 1**, entry 1), while DS is varying from 15 to 45% by increasing the DBU content. This differs from the results reported by Turgut *et al.* who obtained a DS of 48% after 4h for a [PFS]:[DBU] ratio of 1:0.15 with octanethiol [49], or by our group as a DS of 52% was obtained after 10 minutes with a [PFS]:[DBU] ratio of 1:0.2 and by using a perfluorinated thiol [43]. This difference is ascribed to the peculiar structure of MPA that contains two acidic functions with different strength. As the COOH group is a stronger acid than the thiol one is, we can consider that the DBU first reacts with the carboxylic acid groups which does not permit the formation of reaction species if the DBU content is too low [47]. In another set of experiments, a larger content of thiol with respect to PFS units was used. This has a tremendous impact on the extent of modification, as a DS of 100% was obtained after 5 min

with a two-fold excess of DBU. This result can be compared to the results reported by Noy *et al.* [47] with a full conversion of penta-fluorophenyl containing (meth)acrylate in presence of MPA in similar experimental conditions.

Table 1. Para-fluoro-thiol reaction of PPFS with mercaptopropionic acid (MEK, RT).

Entry	Time (min)	[PFS]:[MPA]:[DBU]	DS (%)	θ_{water} (°)	$\Delta\theta_{water}$ (°)
1	360	1:1:0.4	0	101	13
2	960	1:1:0.6	23	—	—
	360		15	—	—
	120		14	—	—
	60		12	—	—
	40		6	—	—
	15		0	—	—
3	360	1:1:0.7	32	96.6°	20.1°
4	30	1:1:0.8	37	—	—
5	30	1:1:1	45	90.9°	20.3
6	10	1:2:1.6	56	91.2°	21.2
7	5	1:2:2	100	91.0°	22.1

We also conducted PFTR with a [PFS units]:[MPA]:[DBU] ratio of 1:1:0.6 in MEK at room temperature in order to tune the DS by kinetic control and thus achieve lower DS in a controlled manner (**Table 1**, entry 2). Indeed, in our previous work dealing with hydrogen-bonded films involving hydroxylated-PPFS prepared by PFTR as H-bond donors, we demonstrated that low DS values (up to 16%) were well-suited to control the thickness of the corresponding films [39]. In the experimental conditions described above, the DS increases regularly such that values from 6 to 15 could be achieved in a timescale of 4h (table 1, entry 2). Water contact angles (θ_{water}), as well as water hysteresis ($\Delta\theta_{water}$) were measured on thin

films prepared by spin-coating PPFS-MPA solutions of various DS onto a silicon wafer. While the θ_{water} of unmodified PPFS is 101° with a $\Delta\theta_{water}$ of around 13°, the θ_{water} of PPFS-MPA-based samples are comparatively lower with higher $\Delta\theta_{water}$ (**Table 1**). These values tend to a plateau for a DS of 40% (at around 91° and 22°, respectively). We can conclude that the interfacial interactions between the carboxylic acid groups of the PPFS-MPA polymer and water are enhanced when the DS increases before reaching a plateau while the hydrophobic character of the PPFS sequence is maintained.

3.2. PPFS-MPA/P4VP complexation properties in solution

The ability of PPFS-MPA and P4VP to develop interactions in solution was investigated. Indeed, upon solution mixing, two polymers may lead to *i*) immiscible blends when no interaction are developed, *ii*) miscible blends (when solution mixture remains transparent but interaction exist after solvent extraction) and *iii*) so-called interpolymer complexes (IPC) when precipitation occurs. Recently, we have demonstrated that systems leading to IPC are the ones which allows for the film formation by Layer by Layer deposition *via* successive dipping in the two different polymer solutions [39]. In order to assess the influence of both the DS and the solvent on the hydrogen bonding ability of PPFS-MPA with a strong H-bond acceptor such as P4VP, solutions of polymers were separately prepared and then mixed together (**Fig. 2**). Indeed, the interaction ability between two polymers (A and B) naturally depends on the number of the interacting moieties per macromolecular chain, but also on the solvent since it results from the balance between polymer A/polymer B interactions, polymer A/solvent interactions, and polymer B/solvent interactions [36].

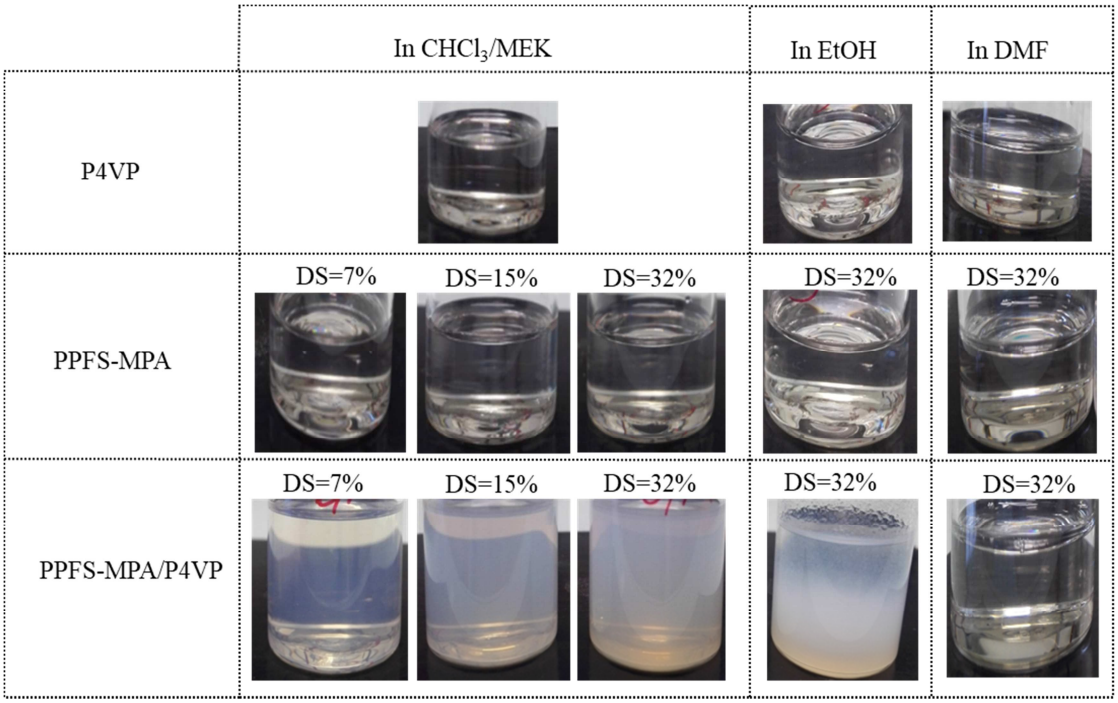

Fig. 2. Images of P4VP, PPFS-MPA (DS = 7%, 15% and 32%) and their mixture (PPFS-MPA/P4VP) in various solvents ($CHCl_3$/MEK, EtOH and DMF) with (COOH):(4VP) molar ratio of 1:6.

Transparent solutions are obtained when the PPFS solution is mixed with P4VP which suggests that no interaction is developed between these two immiscible polymers (data not shown). Three different solvents were used: - a mixed solvent $CHCl_3$/MEK (50/50 vol.), - ethanol, and - DMF. The mixed solvent was employed because PPFS-MPA (for the DS used in this work) is not soluble in chloroform and MEK is not a good solvent for P4VP. Considering that MEK and chloroform are well miscible, such a mixed solvent appeared us as good choice to study the complexation properties in solution. By using $CHCl_3$/MEK as solvent, the PPFS-MPA/P4VP mixtures lead to turbid solutions for all the tested DS (7, 15 and 32%), reflecting the formation of IPC as a consequence of the development of strong interactions between the two polymers that overcome the spontaneous repulsion between them, when PPFS is not chemically modified. This reveals that highly aggregated materials

are formed due to the cooperative effect of interactions, leading to large sequences of associated groups. Moreover, by increasing the DS of PPFS-MPA, the turbidity intensity of the mixture increases probably due to the increase of the extent of the formed IPC. Such an influence of the DS was already reported for PAA/PVA,[29] PMAA/PVA,[29] PAA/PEO[50] and hydroxylated PPFS/P4VP blends [39]. From Fig. 2, it can also be observed that the use of other solvents such as EtOH and DMF influences the complexation ability of PPFS-MPA-32% with P4VP. By using a polar protic solvent such as EtOH, an IPC tends to instantaneously precipitate, indicating that the interactions between the two partners are not only stronger than each polymer/solvent interactions, but also lead to non-solvated and shrunken large aggregates that are more prone to precipitation. Ohno *et al.* [51] obtained similar results by using methanol and ethanol as solvent to study the interactions between PMAA and poly(N-vinyl-pyrrolidone) PVPON. Moreover, Zhunuspayev *et al.* [36] showed that IPC of PAA with PVPON formed in ethanol exhibit two populations of particles at 21 nm and 87 nm. Thus, strong interactions between COOH-containing polymers and H-bonded acceptors are actually not considerably hampered in alcohols used as solvent, that at first might have appeared as a competitive H-bonding donor. A totally different result is obtained upon mixing PPFS-MPA-32% with P4VP in presence of DMF as polar aprotic solvent. Indeed, the solution is transparent (**Fig. 2**). In the latter case, DMF acts as a competitive H-bonding acceptor, as discussed by Dai et *al.* [52] X-ray photoelectron spectroscopy (XPS) was applied to the mixtures after solvent evaporation to identify the nature of the supramolecular interactions developed between PPFS-MPA and P4VP.

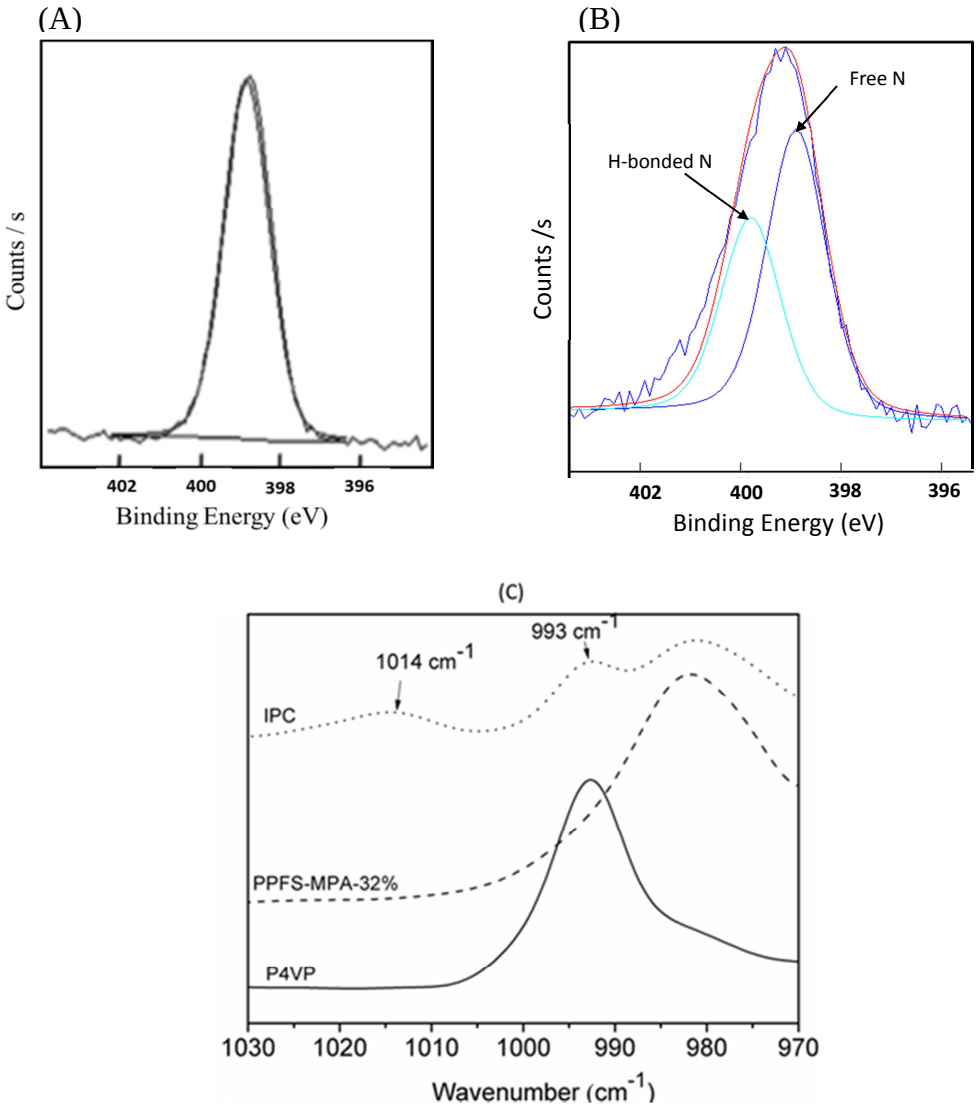

Fig. 3. XPS N1s core-level spectra of (A) P4VP and (B) IPC of PPFS-MPA-32%/P4VP in solid state after solvent evaporation of $CHCl_3$/MEK. (C) ATR FT-IR spectra of P4VP, PPFS-MPA-32 % and IPC of PPFS-MPA-32%/P4VP after solvent evaporation.

In particular, the N1s core-level spectrum collected by XPS reflects the chemical environment of nitrogen when involved in interactions which lowers its electron density. The N1s XPS spectrum of P4VP displays one peak centered at a binding energy (BE) of 398.8 eV (**Fig. 3 (A)**), while a wider peak is obtained for the IPC which can be deconvoluted in two different components: *i*) one that presents the same spectral characteristics than the free Nitrogen, and *ii*) another one centered at a BE of 399.9 eV ascribed to a more electropositive Nitrogen

involved in H-bonds (**Fig. 3 (B)**). We can note that no peak at 401 eV, assigned to positively charged nitrogen is observed in this spectrum, confirming that only H-bonds exist in such IPC [42]. The presence of the two signals visible on the N1s XPS spectrum of P4VP was also highlighted on the patterns related to samples analyzed after the evaporation of ethanol and DMF (**Fig. S2**). Thus, for all mixtures, H-bonds between PPFS-MPA and P4VP are formed. The solvent evaporation induces an increase in the polymer concentration, until the precipitation of the two interacting polymers which are prone to interact themselves through H-bonds. The P4VP/PPFS-MPA mixtures after solvent evaporation were also analyzed by ATR FT-IR, and magnification of the area of interest is presented in **Fig. 3 (C)**. On the spectrum of the IPC, we can observe a peak at 993 cm^{-1}, assigned to the in-plane breath vibration of pyridine ring, and another one at 980 cm^{-1} which stands for the C-F aromatic stretching of PFS ring. The appearance of a new peak at 1014 cm^{-1} is also noticed and is ascribed to the vibration of the pyridine ring involved in H-bonds [40, 42, 53].

3.3. LbL assembly and influence of DS and deposition solvent onto the films features

The ability of PPFS-MPA to develop H-bonds with P4VP was then explored to generate LbL self-assembly films. As evidenced by the studies in solution, the nature of the solvent (separated solvents: $CHCl_3$ and MEK, DMF and ethanol) closely impacts the hydrogen interactions developed between P4VP and PPFS-MPA, by acting on the strength and the extent of aggregated/segregated domains and on the solvation properties. Consequently, it can be anticipated that the solvent used for the deposition assembly will influence the LbL assembly and the corresponding mixtures in solution will be helpful predictors of polymer components to self-assemble into LbL films. Regarding literature, H-bonds mediated films have been mainly prepared in water [19, 25, 29, 31], alcoholic solvents [27, 34, 36], dioxane [36], or mixed solvents (ethanol/DMF [54], ethanol/THF [38]). The influence of the solvent

on the LbL assembly for one given interacting combination [36, 37] especially in the case of water-insoluble carboxylic acid containing polymers has been scarcely reported in literature. Firstly, the sequential multilayer buildup was attempted by successively dip-coating an inorganic substrate (glass slide or silicon wafer) into a solution of P4VP in $CHCl_3$ (2 g/L), and into a solution of PPFS-MPA (7 %, 15 %, and 32 %) in MEK (2 g/L), up to obtain the number of desired bilayers. Indeed, the complexation of P4VP with PPFS-MPA (whatever the DS is) in mixed solvent ($CHCl_3$/MEK) instantaneously and spontaneously led to turbid solutions, as the result of the IPC formation which was shown to be a prerequisite to successfully construct multilayer films by LbL approach [29, 39, 55, 56]. As the two partners implied into the LbL film are chromophores, UV spectroscopy is particularly well-adapted to monitor the film assembly. Thus, UV spectrum was collected at each deposited (P4VP/PPFS-MPA) bilayer. UV absorbance signal resulting from the combination of PPFS-MPA with the lowest DS (7%) and P4VP could hardly be detected, whatever the number of deposited bilayers. This is probably due to the very low amount of deposited polymers and a lack of the UV sensitivity. In contrary, the use of PPFS-MPA-15% and 32 %, combined to P4VP allows for a clear UV response. This proves that the number of interacting groups per polymer chain is a key parameter that governs the assembly process. As an example, Fig. 4 (A) displays UV spectra collected after each deposited (P4VP/PPFS-MPA-15%) bilayer, up to 15 bilayers.

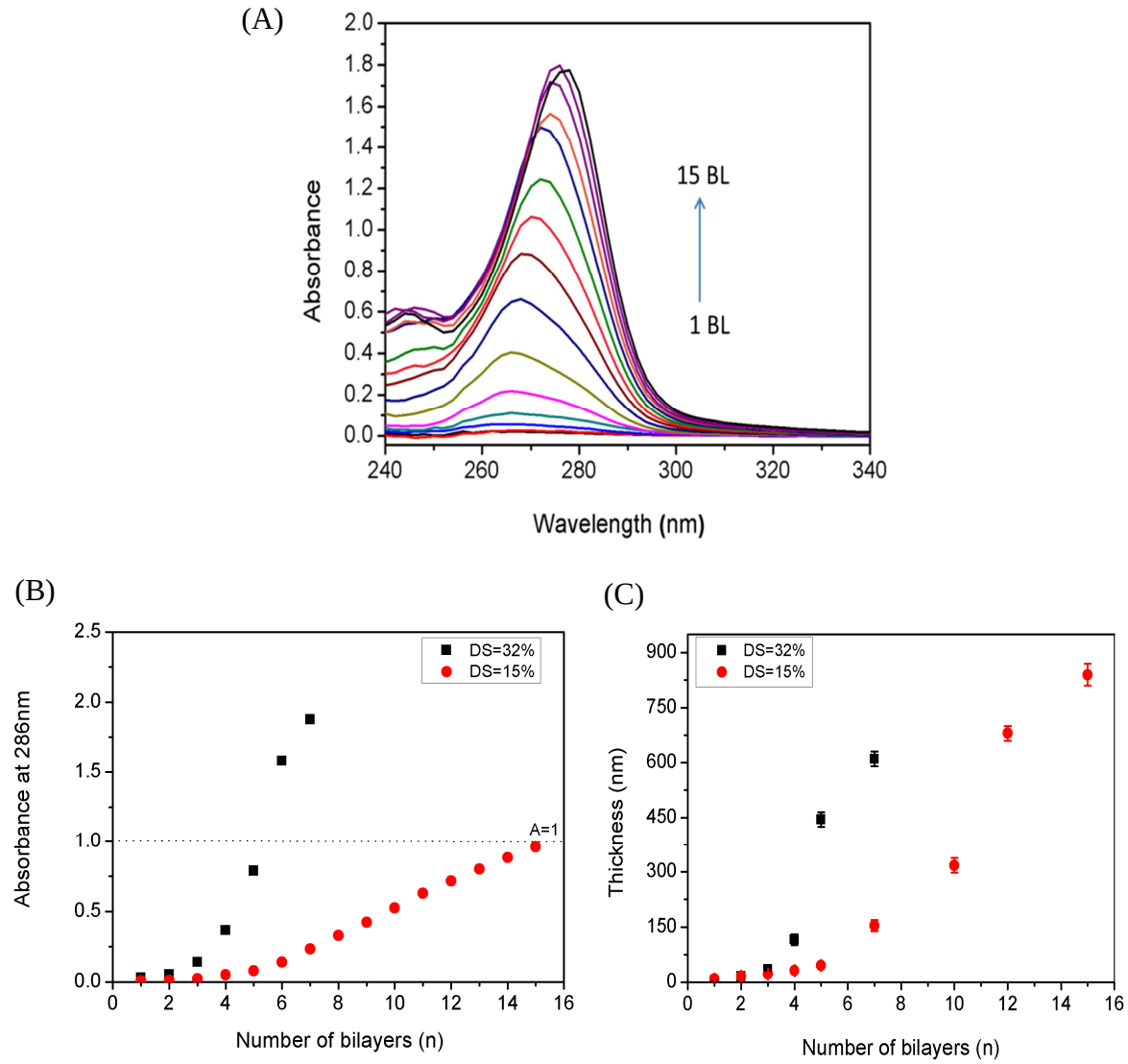

Fig. 4. (A) UV absorbance spectra of $(P4VP/PPFS\text{-}MPA)_n$ ($CHCl_3$ for P4VP and MEK for PPFS-MPA-15%) deposited onto a glass slide. Evolution of (B) the UV absorbance intensity at 286 nm and of (C) the thickness of the film as a function of the number of deposited bilayers, for PPFS-MPA-15% (●) and PPFS-MPA-32% (■).

The gradual increase of the UV absorbance all along the deposition cycle evidences the possibility to utilize PPFS-MPA as H-bond donor partner in conjunction with P4VP to assemble multilayer films in a step by step manner. A similar tendency was observed when using PPFS-MPA-32 % (**Fig. S3**). The presence of an additional peak in the XPS pattern at 399.8 eV (**Fig. S4 (A)**) and the appearance of a new IR absorbance band at 1014 cm^{-1} on the

zoom of the ATR FT-IR spectrum of $(P4VP/PPFSMPA)_n$ in the range of 900-1040 cm^{-1} (**Fig. S4 (B)**) prove that the LbL assembly is driven by the formation of H-bonds between the two interacting polymers. This completely supports the study in solution. In order to gain insight on the growth mechanism and on the impact of the DS of PPFS-MPA, the UV absorbance collected at λ = 286 nm (signature of PPFS-MPA embedded in the film) of the P4VP/PPFS-MPA (DS = 15 and 32%) deposition was typically measured at each deposited bilayer (**Fig. 4 (B)**). The corresponding evolution of the film thickness (measured by AFM after performing a scratch on the surface) was concomitantly analyzed (**Fig. 4 (C)**). Both the UV response and the thickness follow a two-step evolution profile that is shown to be dependent on the DS value of PPFS-MPA. Note that the same conclusion can be drawn from the complementary ATR FT-IR analysis acquired at each deposited bilayer (**Fig. S5**). Whatever the DS is, the assembly growth is non-linear over this range of deposited bilayers and exhibits two successive construction modes: *i*) a quite low deposition regime followed by *ii*) a much higher deposition one from the fourth deposited bilayer. The slope divergence between the two domains suggests different chain organizations at the surface. For low film thicknesses, *i.e.* at the beginning of the construction process corresponding to the first regime, we can suppose that the underlying silicon substrate impacts the films features, and notably the deposition mechanism of the polymers. Above a thickness threshold, the inorganic substrate may be considered as less impactful. Moreover, these two adsorption regimes are probably due to polymer diffusion phenomena which occur inside the film during the immersion steps, and are closely governed by the thickness of the pre-adsorbed polymers (role of reservoir) (see *vide-infra*). Note that most of H-bonded LbL films exhibit only one growth regime (linear or exponential).[24,36,37,54] For PPFS-MPA with DS of 15%, from n = 0 to 4 bilayers, the UV absorbance slightly varies and a low amount of polymer is deposited, resulting in very thin films. From n = 4 bilayers, the thickness noticeably increases for the two DS of PPFS-MPA.

In particular, the use of PPFS-MPA-32% contributes to generate thick films. Indeed, the film constructed from the deposition of 7 bilayers including PPFS-MPA-32 % displays a thickness around 600 nm against 150 nm for the film based on PPFS-MPA-15 %. Such thicknesses measured for (P4VP/PPFS-MPA-32%) are slightly lower than the one of H-bonded LbL assembly of P4VP with hydroxylated-PPFS[39] but remains high compared to most of H-bonds mediated LbL films.[37] These pronounced differences between the two DS of PPFS-MPA suggest different modes of polymer adsorption which are influenced by the number of interacting -COOH moieties per macromolecular chain. The film constructed from high DS tends to assemble with a higher density of active H-bonds developed between sequential deposited layers. The benefit impact of the DS values on the LbL stepwise assembly was already reported in literature, as for instance in the case of stereocomplexation-driven LbL films.[13] This is consistent with the turbidity enhancement observed for mixtures in solution containing high DS of PPFS-MPA. Moreover, the surface features of the (P4VP/PPFS-MPA-15%) film were investigated by AFM (**Fig. 5 (A)**) and by water wettability measurements (**Fig. 5 (B)**). The topography of the deposition of 5, 7 and 15 bilayers leading to a thickness of around 70 nm, 150 nm, and 825 nm, respectively was analyzed (**Fig. 5 (A)**).

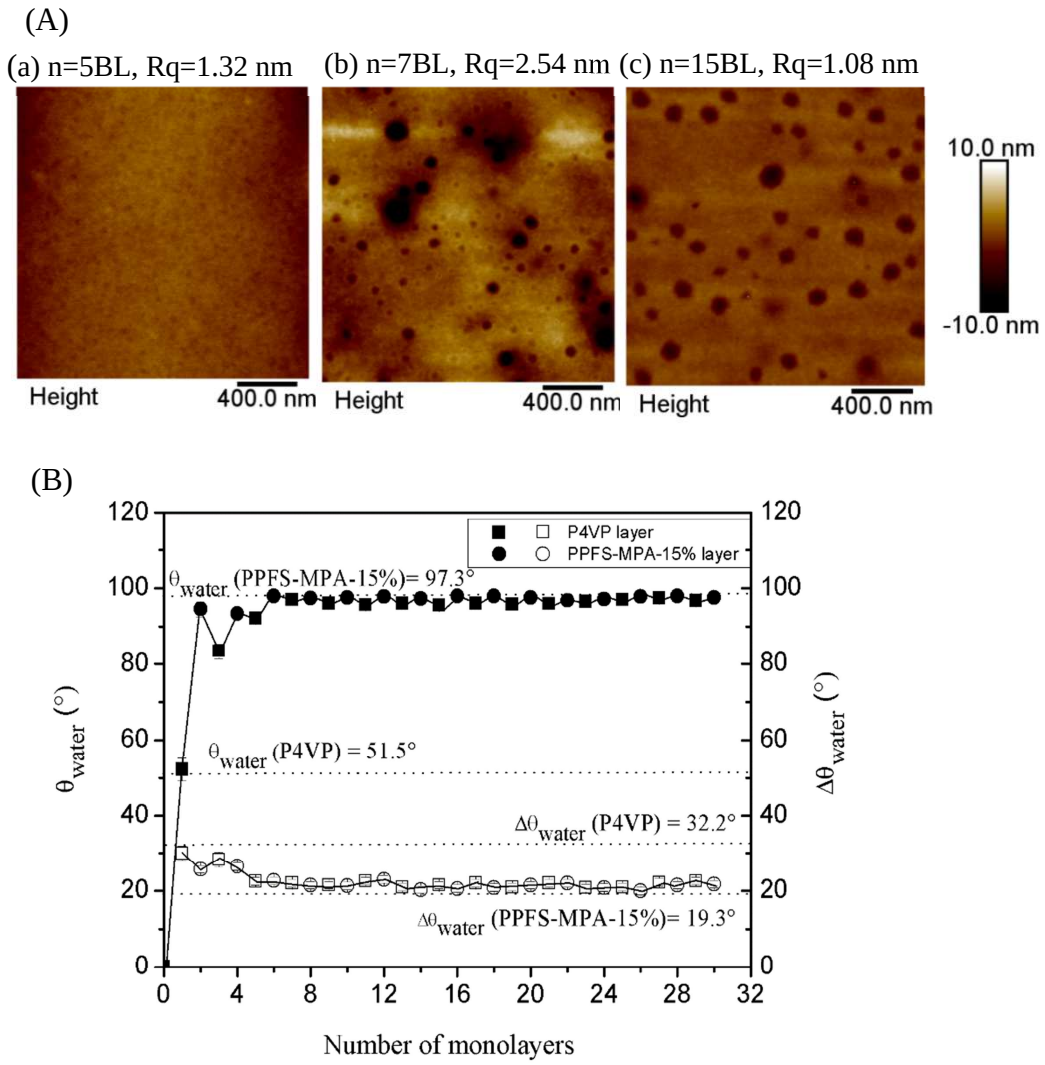

Fig. 5. (A) AFM topography collected after n = 5 (a), 7 (b), 15 (c) deposited bilayers and (B) θ_{water} (filled symbols) and $\Delta\theta_{water}$ (open symbols) of (P4VP/PPFS-MPA)n ($CHCl_3$ for P4VP and MEK for PPFS-MPA-15 %) films measured after each deposited monolayer.

Firstly, we can note that the surface root mean square roughness values (Rq) (see experimental part for more detailed precisions) are relatively low, compared to the thicknesses determined by AFM which confirms that the LbL deposition leads to a covering polymer film. For 5 deposited bilayers, the surface is rather smooth and featureless, while some spherical and polydisperse holes appear for 7 and 15 bilayers resulting in quite nano-porous films. The roughness value is governed by the pore sizes and their distribution along the surface.

However, the surface morphology resulting from the use of PPFS-MPA-32% is smooth and uniform without any defect (**Fig. S6**). It can reasonably be assumed that a lower DS induces a different chain conformation which might act on both the aggregation state of the complexes and the spatial localization of the deposition. Indeed, it is well established that the spatial extent of H-bonded aggregated domains is closely governed by the number of efficient interactions. Moreover, at the beginning of the deposition (n = 2 bilayers) of the film constructed from PPFS-MPA-15%/P4VP, we observed an "island"-type structure by AFM (data not shown), and all along the deposition process, the lateral dimensions of the nodules progressively increase until a more continuous film is formed. Thus, the distance between the neighboring protusions decreases while the area between "islands" is not totally filled, so that regular holes appear within the film.

θ_{water} and $\Delta\theta_{water}$ were measured at each deposited monolayer and are reported in **Fig. 5 (B)**. The θ_{water} and $\Delta\theta_{water}$ of pure P4VP and PPFS-MPA are also provided for comparison. These measurements characterize the first 5-10 A° of the film's outermost surface and are quite sensitive to the chemical composition, the roughness level and the degree of interpenetration of the sequentially adsorbed polymer layers in LbL films.[57] Such water wettability monitoring was exploited to understand the internal organization of LbL films mediated by H-bonds [39], electrostatic interactions [58] or stereocomplexation [13, 59]. After the first immersion into the P4VP solution, θ_{water} increases from a few degrees to 51°, confirming the successful deposition of the P4VP layer. Then, θ_{water} measured after the deposition of PPFS-MPA-15 % is close to a value of 97° suggesting the presence of the more hydrophobic carboxylated-PPFS derivative at the surface. From a threshold number of 8 deposited monolayers, that matches with the beginning of the second growth regime for which the thickness noticeably increases (**Fig. 4 (C)**), the water contact angles attain a constant value around 100° (close to θ_{water} of PPFS-MPA) **(Fig. 5 (B))**. However, despite the immersion of the substrate into the P4VP

solution, this polymer is not detected to the extreme surface (on a scale of a few angstrom) since the experimentally measured water contact angle is much higher (θ_{water} around 100 °) than the one of pure P4VP (θ_{water} = 51.5 °) **(Fig. 5 (B))**. Note that even if no alternate evolution of the water contact angle is observed, the film formation along the stepwise deposition process well occurs, as proved by the increase of the thickness and by the increase of the overall spectroscopic response collected from P4VP, showing that P4VP is incrementally inserted within the film at each deposition cycle (**Fig. 4**). The θ_{water} discrepancy observed between the constant θ_{water} value measured from 8 bilayers and the one of P4VP can be due to *i*) an insufficient coverage of the underneath layer by P4VP and *ii*) a partial diffusion of one given P4VP layer (n) into the sublayers (n-1, n-2, n-3 …) and/or the migration of one given PPFS-MPA underlayer up to the outermost layer, during the immersion steps. The presence of a θ_{water} plateau means that from 4 deposited bilayers, corresponding to a thickness of ~ 50 nm (**Fig. 4 (C)**), the deposited polymers form rather disordered layers composed of interdigitated P4VP and PPFS-MPA segments and the wettability properties are only dictated by the PPFS-MPA derivative. Such a strong chain reorganization implying a high degree of mixing between the adsorbed layers was already observed for films composed of P4VP and PPFS copolymers bearing poly(fluorinated hydroxyl) moieties [39] or poly(acrylic acid) and poly(allyl amine) depending on the pH values [60]. The water hysteresis evolution exhibits a similar profile, characterized by a $\Delta\theta_{water}$ plateau from 7-8 deposited monolayers, which reflects a gain in surface homogeneities (chemical and topography uniformities). The water wettability evolution of the film constructed from a PPFS-MPA-32 % is quite different (**Fig. S6 (B)**). Up to 10 monolayers, the θ_{water} value changes as a function of the deposited layer, and then the amplitude of the θ_{water} oscillation progressively decreases and tends to a steady value. As previously mentioned, the disappearance of the oscillatory trend in θ_{water} reflects the formation of mixed layers.

Moreover, as the film resulting from the use of PPFS-MPA-32 % is noticeably thicker than the one prepared with the lower DS (**Fig. 4 (C)**), it is reasonable to hypothesize that the level of interpenetration depends on the thickness. Indeed, it was shown that the diffusion ability of a preadsorbed polymer depends on the thickness layer deposited at the step (n), compared to the one deposited at the step (n-1) [39, 60]. Furthermore, given that the film generated from DS = 32 % displays a relatively featureless morphology, we can assume that the θ_{water} and $\Delta\theta_{water}$ mainly reflect the chemical changes and not the topographic ones. Then, to investigate the impact of the solvent, the successive deposition of P4VP and PPFS-MPA-32 % was also attempted from solutions in DMF and ethanol, and was analyzed by UV spectroscopy. The UV study shows that no film is formed onto the substrate when DMF is used as deposition solvent (**Fig. S7**). This confirms the study in solution which underpinned the formation of miscible blends, as reflected by the transparency of the solution. DMF is detrimental for the formation of effective and active H-bonds between the two partners. Interactions between PPFS-MPA and DMF seem to predominate and compete with the ones expected with P4VP, thus preventing from the formation of LbL films. This is consistent with our previous work dealing with hydroxylated-PPFS derivatives which demonstrated that the formation of IPC in solution is a required condition to obtain covering LbL films [39]. A similar conclusion was reported for the deposition of PVPON with PAA, for which no film was formed when using aprotic DMSO as solvent, behaving as a hydrogen bonding acceptor [37]. Lastly, the sequential deposition of the polymers dissolved in ethanol was attempted and UV analysis proved the successful formation of films. The UV absorbance at 272 nm (**Fig. 6 (A) and Fig. S8)** and the thickness (**Fig. 6 (B)** of the (P4VP/PPFS-MPA-32 %)n film were quantified after each deposited bilayer. The evolution profiles deeply differ from the growth mechanism resulting from the use of separated solvents ($CHCl_3$ and MEK).

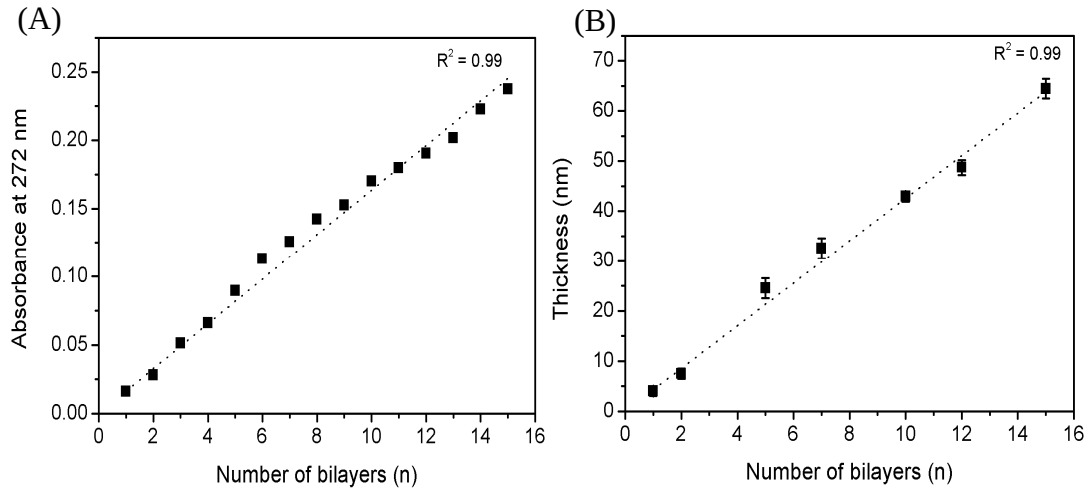

Fig. 6. Evolution of (A) UV absorbance intensity of at 272 nm and (B) thickness of the film as a function of the number of deposited bilayers, for PPFS-MPA-32 % by using ethanol as deposition solvent.

Fig. 6 shows that the absorbance at 272 nm and the thickness follow a quasi-linear increase with the number of deposited bilayers. This linear growth mechanism indicates that a constant increment of polymers is deposited at each deposition cycle. The thickness is around 65 nm for 15 bilayers with an increment per assembling cycle around 4.3 nm. The film obtained from the use of ethanol is much thinner that the ones constructed from the use of two different solvents ($CHCl_3$ for P4VP, and MEK for PPFS-MPA). These thicknesses are particularly low for H-bonded films [37]. This can be reasonably ascribed to the quite compact conformation adopted by the polymer chains in ethanol and by the poor solvation degree of the H-bonded complexes by this solvent. Consequently, we can anticipate that only a few groups (-COOH and pyridine) deposited at a given cycle (n) efficiently interact with the ones belonging to the subsequent layer (n+1), explaining that the amount of deposited polymer is rather low. Moreover, the fluorinated backbone of the PPFS-MPA derivatives is not well solvated by polar ethanol which contributes to restrict its entrapment within the preadsorbed layers during

the immersion. Also, even if precipitates were obtained in solution, we can suppose that ethanol could compete with H-bonds during the deposition which is expected to jeopardize the number of interactions between P4VP and PPFS-MPA, and thus affect the film thickness. Consequently, the thickness is consequently small, contrary to the films resulting from the dipping into $CHCl_3$ for P4VP and MEK for PPFS-MPA. The AFM height images of the LbL films obtained from ethanol with n = 5, 7, and 15 bilayers were collected (**Fig. 7 (A)**), and the water wettability was measured after each deposited monolayer (**Fig. 7 (B)**).

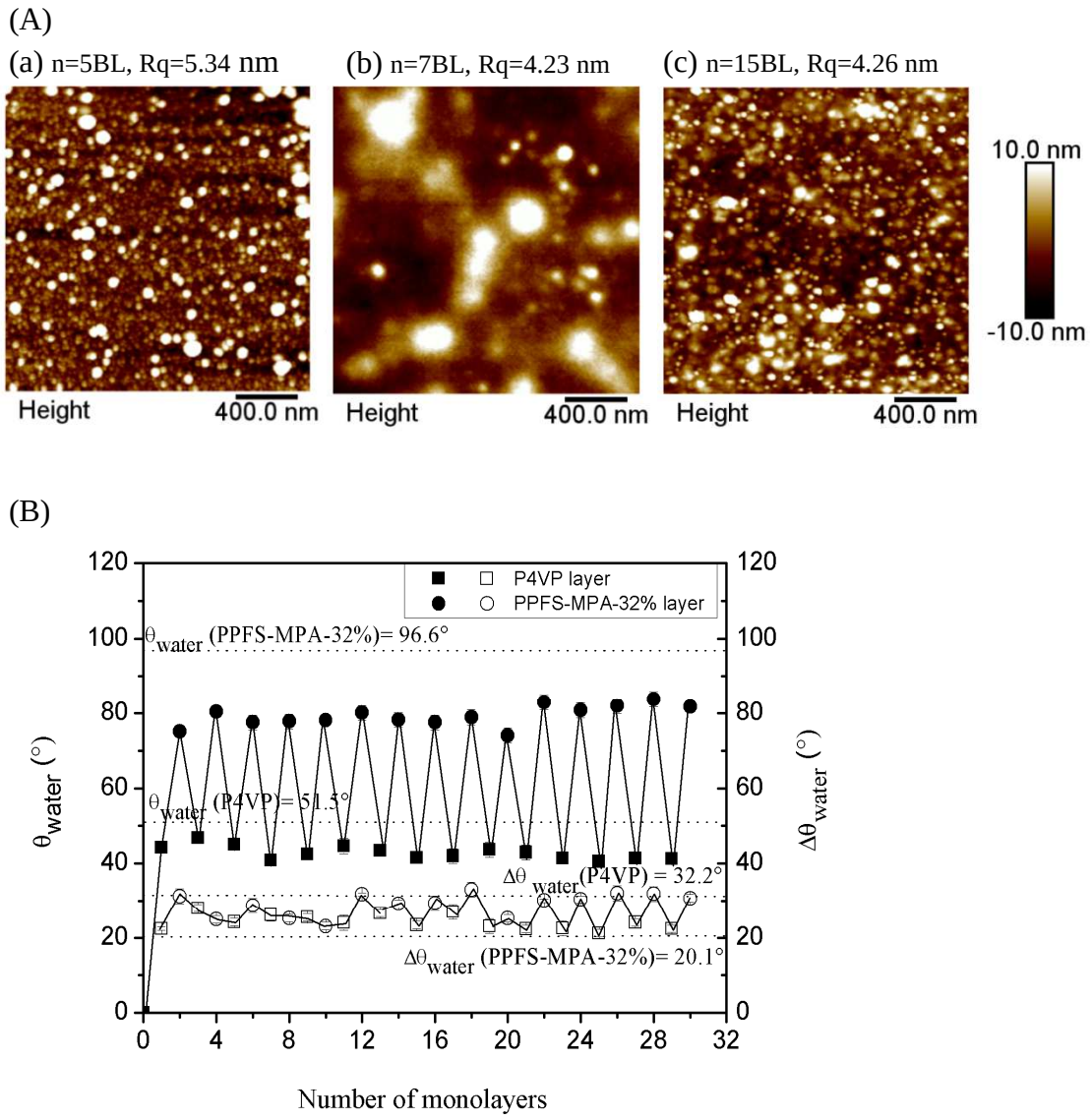

Fig. 7. (A) AFM topography collected after n = 5 (a), 7(b), 15(c) deposited bilayers and (B) θ_{water} (filled symbols) and $\Delta\theta_{water}$ (open symbols) of (P4VP/PPFS-MPA-32 %)n (ethanol)

films measured after each deposited monolayer.

AFM imaging reveals patchy morphologies with the presence of rather spherical polydisperse nanometric dots irregularly distributed along the surface which induce a quite higher value of roughness (around 4-5 nm). The coacervates present at the surface are probably constituted of multiple aggregated polymers. The low amount of deposited P4VP and PPFS-MPA, when ethanol is used as deposition solvent contributes to generate such a nodular morphology. Moreover, these nano-islets may originate from the strongly associated state of partners adopting a packed conformation induced by ethanol. This is consistent with the appearance of precipitates in ethanol upon mixing of P4VP with PPFS-MPA-32 %, as a consequence of a strong aggregation and a low solvation of the H-bonded domains by this polar protic solvent. Regarding the wettability measurements, the θ_{water} increases up to 45° and 75° after the first deposition of P4VP and PPFS-MPA, respectively. These values are much lower than the θ_{water} measured for pure P4VP and PPFS-MPA, which can be ascribed to the effect of the underlying silicon substrate. Afterward, a well distinct periodic oscillation, dependent on the nature of the outermost layer, is observed. The θ_{water} values measured at each cycle are well reproducible and are dependent on the outermost adsorbed layer. Meanwhile, none of θ_{water} values reach the one of the corresponding pure polymer, leading to rather hydrophilic films ($\theta_{water} < 90°$). This discrepancy can be caused by the peculiar embossed surface morphology and by the surface roughness, as underpinned by the AFM height images. The presence of such θ_{water} alternative variation demonstrates that the deposition from ethanol solutions allows for the formation of well-stratified layers, almost compartmentalized and composed of individual interacting partner layer, compared to the films obtained by the deposition of P4VP in $CHCl_3$ and PPFS-MPA in MEK for which a high degree of interpenetration was highlighted. The use of ethanol much probably restricts the diffusion of

both PPFS-MPA and P4VP which quite limits the chain rearrangement and reduces the internal interfacial mixing.

These results and the different behaviors evidence that the solvent plays a key and tremendous role on *i*) the growth mechanism (one or two linear segments), *ii*) the thickness (from a few tens of nm for the use of ethanol up to a few hundred of nm for the use of separated solvents), *iii)* the internal organization (compartmentalized layers or strongly interpenetrated layers), and *iv*) the surface features, in terms of topography (smooth, or patchy morphology), and water wettability properties (hydrophobic or hydrophilic character). Indeed, the nature of the solvent (herein $CHCl_3$, MEK, ethanol, and DMF) influences *i*) the solvation state and the conformation of the polymer chains in solution as well as the ones of the more outermost layers deposited on pre-adsorbed polymers, *ii*) the balance between the polymer A/ solvent, the polymer B/solvent and the polymer A/polymer B interactions, and *iii*) the solvation level of the H-bonded domains. The link between the conformation chain in solution and the features of the LbL assembly was reported in literature, for instance by Ma et *al.* for films composed of poly(vinylpyrrolidone) and poly(acrylic acid) [37] and by Chen *et al.* [38] who studied polyacrylate-containing films constructed from solvents with different compositions. In particular, Ma *et al.* [37] showed that polymer-solvent interactions must be overcome to obtain hydrogen-bonded complexes. The authors demonstrated that dimethylacetamide, tetramethylurea, dimethylsulfoxide and *N*-methyl pyrrolidone strongly interact with the polymers (PAA and PVPON), and thus no LbL films can be formed, which is not the case when using acidic water and alcoholic solvents. Also, they evidenced that a polymer under a compact conformation in a given solvent leads to rough films, related to a lower accessibility to the interacting sites. Chen *et al.* [38] showed that the assembling process is closely impacted by the size of polymer coil in solution and an extended conformation tends to decrease the adsorbed amount.

Consequently, the solvent controls the availability and the accessibility of the interacting sites between two adjacent deposited layers, the degree of compactness of the H-bonded complexes and governs the diffusion ability (and the reorganization) of the embedded polymers inside the film during the immersion steps. Further works are in progress to gain insight on the dynamic of individual polymer chains (P4VP and PPFS-MPA), and the H-bonded complexes in solution.

4. Conclusion

Carboxylated-PPFS derivatives were prepared through the versatile and efficient para-fluoro thiol reaction with mercaptopropionic acid. The PPFS modification was shown to be chemoselective and the extent of the PPFS modification was adjusted by tuning the experimental parameters (DS from 7 to 100 %). From the investigation of mixtures of PPFS-MPA with P4VP in solution, it results that the miscibility between PPFS and P4VP is enhanced by the presence of carboxylic acid groups, as the consequence of the formation H-bonded complexes. Interpolymer complexes leading to turbid solutions were generated in mixed solvent ($CHCl_3$/MEK) and in ethanol, while using DMF leads to a transparent solution. Besides, the ability of these PPFS-MPA derivatives to develop H-bonds with P4VP was exploited to construct LbL self-assembly films. The feasibility to prepare thin films by successive dipping steps was evidenced and it appeared that the driving forces of the film formation are H-bonds developed between the two partners. The influence of the DS of PPFS-MPA and the nature of solvent was carefully investigated. Increasing the DS value contributes to increase the amount of deposited polymer and thus the resulting thickness, related to the enhancement of H-bonds formed at each assembly step. Interestingly, as predicted by the study of PPFS-MPA/P4VP mixtures in solution, the nature of the solvent deposition strongly influences the characteristics of LbL films, by directly affecting the H-bonds developed between the two interacting partners. By acting as a competitor solvent, DMF does not allow

for the formation of LbL films. The deposition from separated solvents ($CHCl_3$ for P4VP, MEK for PPFS-MPA) leads to thick and well-covering films constructed through a two-step growth mechanism. The LbL film presents a high level of segmental interpenetration between alternating layers and the resulting surface morphology is quite smooth and featureless. In comparison, the deposition from ethanol solution leads to well-stratified and very thin films by following a linear growth construction. Moreover, the films exhibit an uneven and patchy topography, yielding a relatively high roughness. Thus, changing the solvent deposition appears as powerful manner to generate tailor-made films with tunable surface properties, for a given set of partners.

Conflicts of interest

None.

Acknowledgments

The authors thank the NMR Polymer Centre of "Institut de Chimie de Lyon" (FR 3023) for access to NMR facilities and helpful comments and they thank Sébastien Pruvost (IMP, UMR 5223, Villeurbanne) for his helpful suggestion in the AFM analysis.

Funding

The China Scholarship Council (CSC) is warmly acknowledged for Q.Y. Ph.D's grant.

Supporting information available

^{19}F-NMR spectrum of PPFS and PPFS-MPA-32%, XPS N1s core-level spectra of IPC and miscible polymer mixtures from EtOH and DMF, XPS N1s spectrum and ATR FT-IR spectrum of (P4VP/PPFS-MPA)n (use of separated solvents), Evolution of ATR FT-IR

absorbance at 1597 cm^{-1} for P4VP as a function of the number of deposited bilayers (by using separated solvents), AFM images collected after 5 and 7 deposited bilayers and θ_{water} and $\Delta\theta_{water}$ of (P4VP/PPFS-MPA)n (separated solvents) measured after each deposited monolayer, UV absorbance spectra of (P4VP/PPFS-MPA-32 %)n (DMF).

References

[1] Li, Y.; Wang, X.; Sun, J. Layer-by-layer assembly for rapid fabrication of thick polymeric films. Chem. Soc. Rev. 41 **(**2012) 5998-6009.

[2] G. Decher, J.B. Schlenoff, Eds. in Multilayer thin films: Sequential Assembly of Nanocomposite Materials 2003, Wiley-VCH, Weinheim, Germany.

[3] Richardson, J.J.; Cui, J.; Björnmalm, M.; Braunger, J.A.; Ejima, H.; Caruso, F. Innovation in Layer-by-Layer Assembly. Chem. Rev. 116 (2016) 14828-14867.

[4] Ariga, K.; Yamauchi, Y.; Rydzek, G.; Ji, Q.; Yonamine, Y.; Wu, K. C-W.; Hill, J.P. Layer-by-layer Nanoarchitectonics: Invention, Innovation, and Evolution. Chem. Lett. 43 (2014) 36-68.

[5] Xiao, F-X.; Pagliaro, M.; Xu, X-J.; Liu, B. Layer-by-layer assembly of versatile nanoarchitectures with diverse dimensionality: a new perspective for rational construction of multilayer assemblies**.** Chem. Soc. Rev**.** 45 (2016) 3088-3121**.**

[6] Yoshida, K.; Hasebe, Y.; Takahashi, S.; Sato, K.; Anzai, J-i. Layer-by-layer deposited nano- and micro-assemblies for insulin delivery: A review. Mater. Sci. Eng. C 34 (2014) 384-392.

[7] Charlot, A.; Sciannaméa, V.; Lenoir, S.; Faure, E.; Jérôme, R.; Jérôme, C.; Van De Weerdt, C.; Martial, J.; Archambeau, C.; Willet, N.; Duwez, A.-S.;. Fustin, C.-A; Detrembleur, C. All-in-one strategy for the fabrication of antimicrobial biomimetic films on stainless steel. J. Mater. Chem. 19 (2009) 4117-4125.

[8] Qiu, X.; Li, Z.; Li, X.; Zhang, Z. Flame retardant coatings prepared using layer by layer assembly: A review. Chemical Engineering Journal. 334 (2018) 108-122.

[9] Tang, Z.; Wang, Y.; Podsiadlo, P.; Kotov, N. A. Biomedical Applications of Layer-by-Layer Assembly: From Biomimetics to Tissue Engineering, Adv. Mater. 18 (2006) 3203-3224.

[10] Zhang, S.; Xing, M; Li, B. Biomimetic Layer-by-Layer Self-Assembly of Nanofilms, Nanocoatings, and 3D Scaffolds for Tissue Engineering. International Journal of Molecular Sciences 19 (2018) 1641.

[11] Wang, K. Naka, H. Itoh, T. Uemura and Y. Chujo, Preparation of Oriented Ultrathin Films via Self-Assembly Based on Charge Transfer Interaction between π-Conjugated Poly(dithiafulvene) and Acceptor Polymer. Macromolecules 36 (2003) 533-535.

[12] Crespo-Biel, O.; Dordi, B.; Reinhoudt, D.N.; Huskens, J. Supramolecular Layer-by-Layer Assembly: Alternating Adsorptions of Guest- and Host-Functionalized Molecules and Particles Using Multivalent Supramolecular Interactions. J. Am. Chem. Soc. 127 (2005) 7594-7600.

[13] Bahloul, M.; Pruvost, S.; Fleury, E.; Portinha, D.; Charlot, A. Dip- and spin-assisted stereocomplexation-driven LbL self-assembly involving homochiral PVA-g-OLLA and PVA-g-ODLA copolymers. RSC Advances 5 (2015) 107370-107377.

[14] Decher, G. Fuzzy Nanoassemblies: Toward Layered Polymeric Multicomposites. Science 277 (1997) 1232-1237.

[15] Kelly, K.D.; Fares, H.M.; Abou Shaheen, S.; Schlenoff, J.B. Intrinsic Properties of Polyelectrolyte Multilayer Membranes: Erasing the Memory of the Interface. Langmuir 34 (2018) 3874-3883.

[16] Castelnovo, M.; Joanny, J-F. Formation of Polyelectrolyte Multilayers. Langmuir 16 (2000) 7524-7532.

[17] Zahn, R.; Vörös, J.; Zambelli, T. Tuning the Electrochemical Swelling of Polyelectrolyte Multilayers toward Nanoactuation. Langmuir 30 (2014) 12057-12066.

[18] Erel, I.; Karahan, H.E.; Tuncer, C.; Bütün, V.; Demirel, A.L. Hydrogen-bonded multilayers of micelles of a dually responsive dicationic block copolymer. Soft Matter 8 (2012) 827-836.

[19] Kharlampieva, E.; Sukhishvili, S. A. Hydrogen-bonded Layer-by-Layer Polymer films. Journal of Macromolecular Science, Part C: Polymer reviews 46 (2006) 377-395.

[20] Such, G. K.; Johnston, A. P. R.; Caruso, F. Engineered Hydrogen-Bonded Polymer Multilayers: from Assembly to Biomedical Applications. Chem. Soc. Rev. 40 (2011), 19-29

[21] Kuo, S.; Chan, S.; Chang, F. Effect of Hydrogen Bonding Strength on the Microstructure and Crystallization Behavior of Crystalline Polymer Blends. Macromolecules 55 (2003) 6653-6661.

[22] Takemoto, Y.; Ajiro, H.; Akashi, M. Hydrogen-bonded multilayers films based on poly(N-vinylamide) derivatives and tannic acid. Langmuir 31 (2015) 6863-6869.

[23] Kaminski, G. A. T.; Sierakowski, M. R.; Pontarolo, R.; Santos, L. A. D; Freitas, R. A. D. Layer-by-Layer Polysaccharide-Coated Liposomes for Sustained Delivery of Epidermal Growth Factor. Carbohydr. Polym. 140 (2016) 129-135.

[24] Deng, Y.; Wang, T.; Guo, Y.; Qiu, X.; Qian, Y. Layer-by-Layer self-assembled films of a lignin-based polymer through hydrogen bonding. ACS Sus. Chem. Eng. 3 (2015) 1215-1220.

[25] Cheung, J.H.; Stockton, W.B.; Rubner, M. F. Molecular-Level Processing of Conjugated Polymers. 4. Layer-by-Layer Manipulation of Polyaniline via Hydrogen-Bonding Interactions. Macromolecules 30 (1997) 2712-2716.

[26] Sun, J.; Li, J.; Liu, D.; Ma, Y.; Yang, S. pH-Responsive Janus Film Constructed with Hydrogen-Bonding Assembly and Dopamine Chemistry, Langmuir, 34 (2018) 6653-6659

[27] Wang, L., Wang, Z., Zhang, X., Shen, J., Chi, L., Fuchs, H. A new approach for the fabrication of an alternating multilayer film of poly(4-vinyl pyridine) and poly(acrylic acid) based on hydrogen bonding. Macromol. Rapid Commun. 18 (1997) 509-514.

[28] Zhuk, A.; Pavlukhina, S.; Sukhishvili, S.A., Hydrogen-Bonded Layer-by-Layer Temperature-Triggered Release Films. Langmuir 25 (2009) 14025-14029.

[29] Lee, H., Mensire, R., Cohen, R.E., Ruibner, M. F. Strategies for hydrogen bonding Layer-by-layer Assembly of poly(vinyl alcohol) with weak polyacids. Macromolecules 45 (2012) 347-355.

[30] Li, Y.; Pan, T.; Ma, B.; Liu, J.; Sun, J. Healable Antifouling Films Composed of Partially Hydrolyzed Poly(2-Ethyl-2-Oxazoline) and Poly(acrylic Acid). ACS Appl. Mater. Interfaces 9 (2017) 14429–14436.

[31] deLongchamp, D. M.; Hammond, P.T. Highly ion conductive poly(ethylene oxide)-based solid polymer electrolytes from hydrogen bonding layer-by-layer assembly. Langmuir 20 (2004) 5403-5411.

[32] Cui, M.; Lee, P. S. Solid Polymer Electrolyte with High Ionic Conductivity via Layer-by-Layer Deposition. Chem. Mater. 28 (2016) 2934–2940.

[33] Sung, C.; Vidyasagar, A.; Hearn, K.; Lutkenhaus, J.L. Effect of Thickness on the Thermal Properties of Hydrogen-Bonded LbL Assemblies. Langmuir 28 (2012) 8100-8109.

[34] Zhang, H.; Fu, Y.; Wang, D.; Wang, L.; Wang, Z.; Zhang, X. Hydrogen-Bonding-Directed Layer-by-Layer Assembly of Dendrimer and poly(4-Vinylpyridine) and Micropore Formation by Post-Base Treatment. Langmuir 19 (2003) 8497–8502.

[35] Fu, Y.; Bai, S.; Cui, S.; Qiu, D.; Wang, Z.; Zhang, X. Hydrogen-Bonding-Directed Layer-by-Layer Multilayer Assembly: Reconformation Yielding Microporous Films. Macromolecules 35 (2002) 9451-9458.

[36] Zhunuspayev, D. E.; Mun, G. A.; Hole, P.; Khutoryanskiy, V. V. Solvent Effects on the Formation of Nanoparticles and Multilayered Coatings Based on Hydrogen-Bonded Interpolymer Complexes of Poly(Acrylic Acid) with Homo- and Copolymers of N -Vinyl Pyrrolidone. Langmuir 24 (2008) 13742-13747.

[37] Ma, S.; Yuan, Q.; Zhang, X.; Yang, S.; Xu, J. Solvent Effect on Hydrogen-Bonded Thin Film of Poly(vinylpyrrolidone) and Poly(acrylic Acid) Prepared by Layer-by-Layer Assembly. Colloids Surfaces A Physicochem. Eng. Asp. 471 (2015) 11-18.

[38] Chen, Q.; Ma, N.; Qian, H.; Wang, L.; Lu, Z. Layer-by-Layer Assembly of Two Polyacrylate Derivatives: Effect of Solvent Composition and Side-Chain Structure. Polymer. 48 (2007) 2659-2664.

[39] Chen, J.; Duchet, J.; Portinha, D.; Charlot, A. Layer by Layer H-Bonded Assembly of P4VP with Various Hydroxylated PPFS: Impact of the Donor Strength on Growth Mechanism and Surface Features. Langmuir 30 (2014) 10740-10750.

[40] Chen, J.; Dumas, L.; Duchet-Rumeau, J.; Fleury, E.; Charlot, A.; Portinha, D. Tuning H-bond Capability of Hydroxylated-Poly(2,3,4,5,6-pentafluorostyrene) Grafted Copolymers Prepared by Chemoselective and Versatile Thiol-*para*-fluoro “Click-type” Coupling with Mercaptoalcohols. J. Polym. Sci., Part A: Polym. Chem. 50 (2012) 3452-3460.

[41] Dumas, L.; Fleury, E.; Portinha, D. Wettability adjustment of PVDF surfaces by combining radiation-induced grafting of (2,3,4,5,6)-pentafluorostyrene and subsequent chemoselective “click-type” reaction. Polymer, 55 (2014) 2628-2634.

[42] Chen, J.; Vuluga, D.; Crousse, B.; Legros, J.; Duchet-Rumeau, J.; Charlot, A.;

Portinha, D. Polyfluorinated Mercaptoalcohol as a H-bond Modifier of Poly(2,3,4,5,6-pentafluorostyrene) (PPFS) Enhancing Miscibility of Hydroxylated-PPFS with Various Acceptor Polymers. Polymer 54 (2013) 3757-3766.

[43] Yin, Q., Alcouffe, P., Beyou, E., Charlot, A., Portinha, D. Controlled perfluorination of poly(2,3,4,5,6-pentafluorostyrene) (PPFS) and PPFS-functionalized fumed silica by thiol-para-fluoro coupling: Towards the design of self-cleaning (nano)composite films. European Polymer Journal 102 (2018) 120–129.

[44] Delaittre, G.; Barner, L. The para-fluoro-thiol reaction as an efficient tool in polymer chemsitry. Polym. Chem.9 (2018) 2679-2684.

[45] Agar, S.; Baysak, E.; Hizal, G.; Tunca, U.; Durmaz, H. An emerging post-polymerization modification technique : The promise of thiol-para-fluoro click recation. J. Polym. Sci., Part A: Polym. Chem. 56 (2018) 1181-1198.

[46] Valtola, L.; Karesoja, M.; Tenhu, H.; Ihalainen, P.; Sarfraz, J.; Peltonen, J.; Malinen, M.; Urtti, A.; Hietala, S. Breath figure templated semifluorinated block copolymers with tunable surface properties and binding capabilities. J. Appl. Polym. Sci. 132 (2015), 41225.

[47] Noy, J-M.; Koldevitz, M.; Roth, P.J. Thiol-reactive functional poly(meth)acrylates: multicomponent monomer synthesis, RAFT (co)polymerization and highly efficient thiol-*para*-fluoro postpolymerization modification. Polym. Chem. 6 (2015) 436-447

[48] Noy, J.-M.; Friedrich, A.; Batten, K.; Bhebhe, M.M.; Busatto, N.; Batchelor, R.R.; Kristanti, A.; Pei, Y.; Roth, P.J. *Para*-Fluoro Post-polymerization Chemistry of Poly(pentafluorobenzyl methacrylate): Modification with Amines, Thiols, and Carbonylthiolates. Macromolecules, 50 (2017) 7028-7040.

[49] Turgut, H.; Delaittre, G. On the Orthogonality of Two Thiol-Based Modular Ligations. Chem. Eur. J. 22 (2016) 1511-1521.

[50] Chen, Y.; Pang, Y.; Wu, J.; Su, Y.; Liu, J.; Wang, R.; Zhu, B.; Yao, Y.; Yan, D.; Zhu, X.; et al. Controlling the Particle Size of Interpolymer Complexes through Host-Guest Interaction for Drug Delivery. Langmuir 26 (2010) 9011-9016.

[51] Ohno, H.; Abe, K.; Tsuchida, E. Solvent Effect on the Formation of Poly(methacrylic acid)-poly(N-vinyl-2-pyrrolidone) Complex through Hydrogen Bonding. Die Makromol. Chemie 179 (1978) 755-763.

[52] Dai, J; Goh, S. H.; Lee, S. Y. and Siow. K. S. Interpolymer Complexation between Poly(p-Vinylphenol) and Pyridine-Containing Polymers. Polym. J. 26 (1994) 905-911

[53] Ruokolainen, J.; ten Brinke G.; Ikkala, O.; Torkkeli, M.; Serimaa, R. Mesomorphic Structures in Flexible Polymer-Surfactant Systems Due to Hydrogen Bonding: Poly(4-vinylpyridine)-Pentadecylphenol. Macromolecules 29 (1996) 3409-3415.

[54] Zhang, H.; Wang, Z.; Zhang, Y.; Zhang, X. Hydrogen-Bonding-Directed Layer-by-Layer Assembly of Poly (4-Vinylpyridine) and Poly (4-Vinylphenol): Effect of Solvent Composition on Multilayer Buildup. Langmuir 20 (2004) 9366–9370.

[55] Mjahed, H.; Jean-Claude Voegel, J-C.; Armelle Chassepot, A.; Senger, B.; Schaaf, P.; Boulmedais, F. ; Ball, V. Turbidity diagrams of polyanion/polycation complexes in solution as a potential tool to predict the occurrence of polyelectrolyte multilayer deposition. J. Coll. Interf. Sci. 346 (2010) 163-171.

[56] Izumrudov, V.; Kharlampieva, E.; Sukhishvili S.A. Salt-Induced Multilayer Growth: Correlation with Phase Separation in Solution. Macromolecules 37 (2004) 8400-8406.

[57] Quinn, A.; Tjipto, E.; Yu, A.; Gengenbach, T. R.; Caruso, F. Polyelectrolyte Blend Multilayer Films: Surface Morphology, Wettability, and Protein Adsorption Characteristics. Langmuir 23 (2007) 4944-4949.

[58] An, M.; Hong, J.D. Surface modification of hafnia with polyelectrolytes based on the spin-coating electrostatic self-assembly method. Colloids surf A: Physiochem. Eng.

Aspects 348 (2009) 301-304.

[59] Serizawa, T.; Hamada, K.-I., Kitayama, T.; Fujimoto, N.; Hatada, K.; Akashi, M. Stepwise Stereocomplex Assembly of Stereoregular Poly(methyl methacrylate)s on a Substrate. J. Am. Chem. Soc. 122 (2000) 1891-1899.

[60] Yoo, D., Shiratori, S.S., Rubner, M.F. Controlling bilayer composition and surface wettability of sequentially adsorbed multilayers of weak polyelectrolytes. Macromolecules 31 (1998) 4309-4318.

SUPPORTING INFORMATION

Tuning Features of H-bonded Layer by Layer assembly of poly(4-vinyl pyridine) and carboxylated poly-(2,3,4,5,6-pentafluorostyrene) synthesized through para-fluoro-thiol reaction

Quanyi Yin [a,b], Emmanuel Beyou [b], Daniel Portinha [a*], Aurélia Charlot [a*]

[a] Université de Lyon, INSA-Lyon, UMR CNRS 5223, Ingénierie des Matériaux Polymères, F-69622 Villeurbanne Cedex, France

[b] Université de Lyon, Université Lyon 1, UMR CNRS 5223, Ingénierie des Matériaux Polymères, F-69622 Villeurbanne Cedex, France

Corresponding authors: Tel.: +33 4 72 43 63 38; fax: +33 4 72 43 85 27.

E-mail addresses: **daniel.portinha@insa-lyon.fr, aurelia.charlot@insa-lyon.fr**

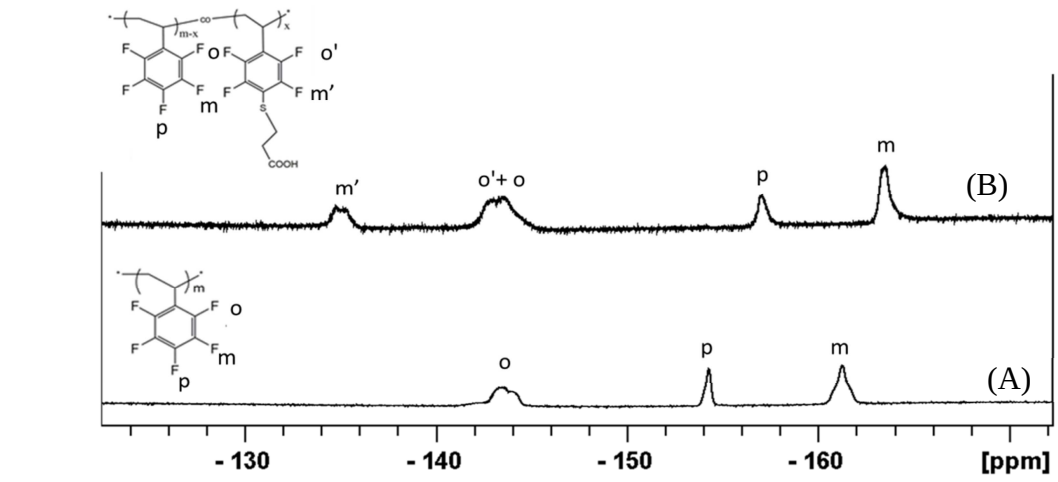

Fig. S1. ^{19}F-NMR spectrum of (A) PPFS and (B) PPFS-MPA-32%.

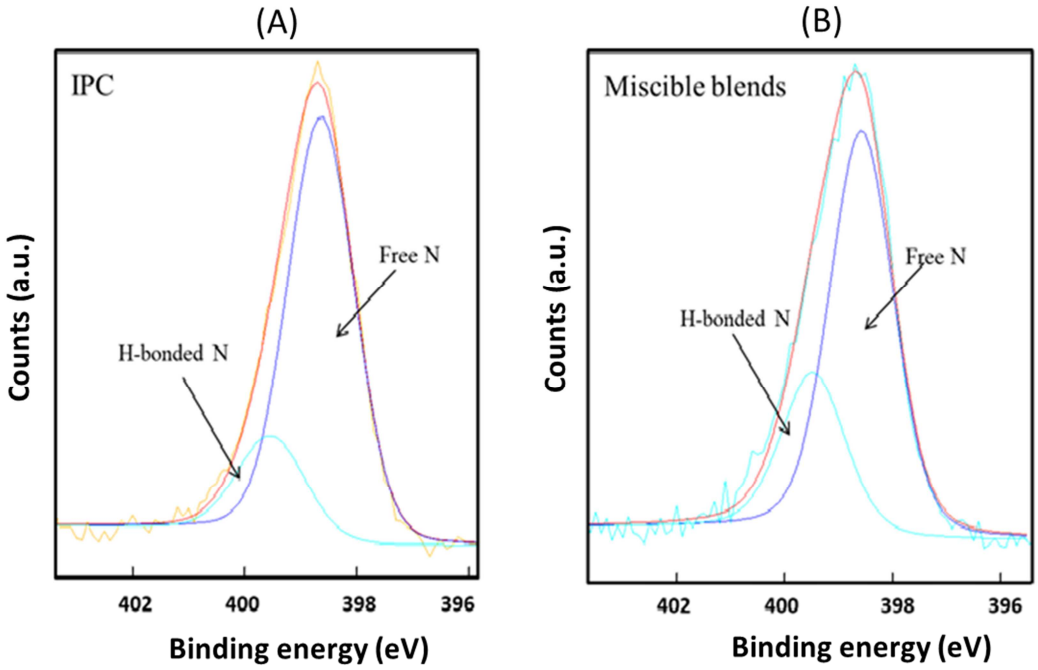

Fig. S2. XPS N1s core-level spectra of (A) IPC and (B) miscible polymer mixtures of PPFS-MPA-32%/P4VP in solid state after solvent evaporation from EtOH and DMF, respectively.

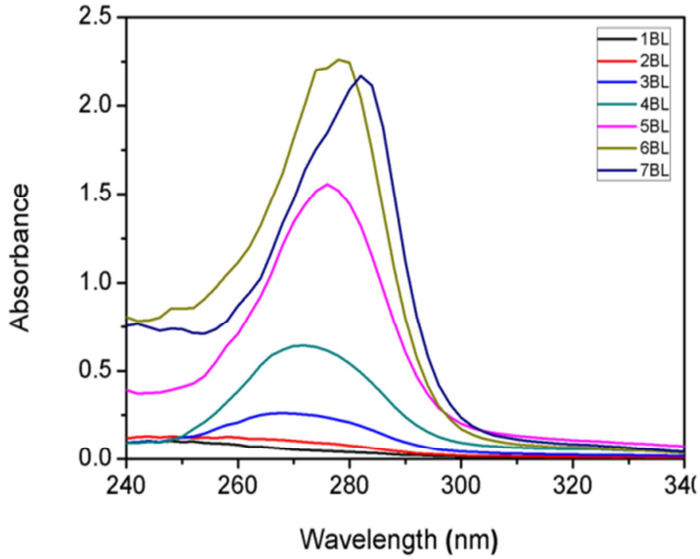

Fig. S3. UV absorbance spectra of $(P4VP/PPFS\text{-}MPA)_n$ ($CHCl_3$ for P4VP and MEK for PPFS-MPA-32%) deposited onto a glass slide.

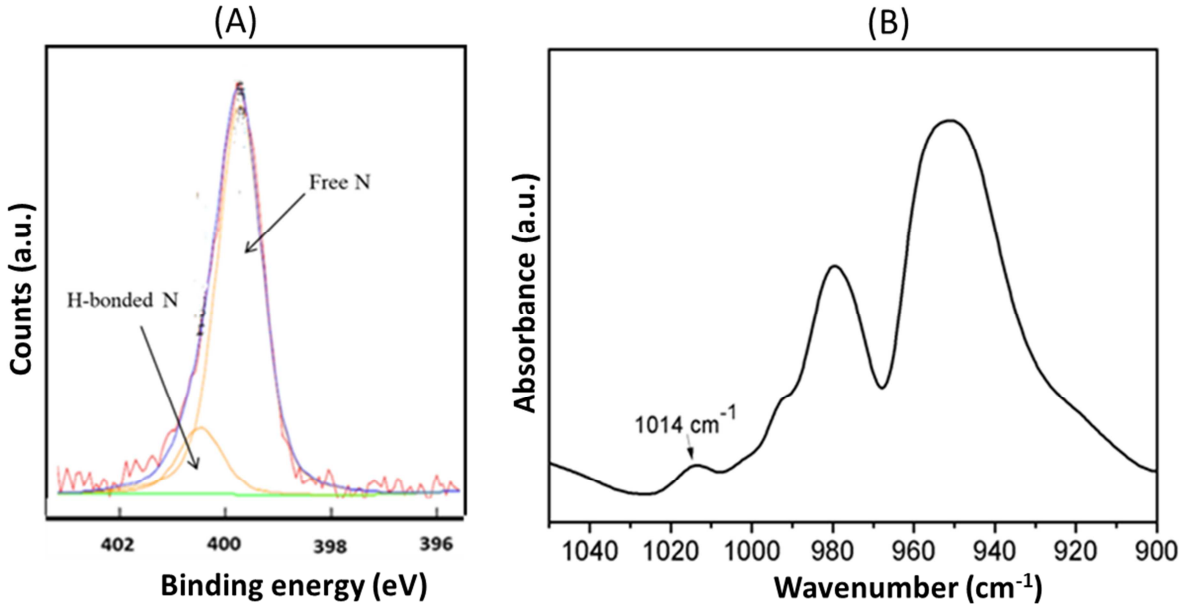

Fig. S4. (A) XPS N1s spectrum and (B) ATR FT-IR spectrum of (P4VP/PPFS-MPA)n ($CHCl_3$ for P4VP and MEK for PPFS-MPA-32%, c = 2 g/L) (n = 7 BL).

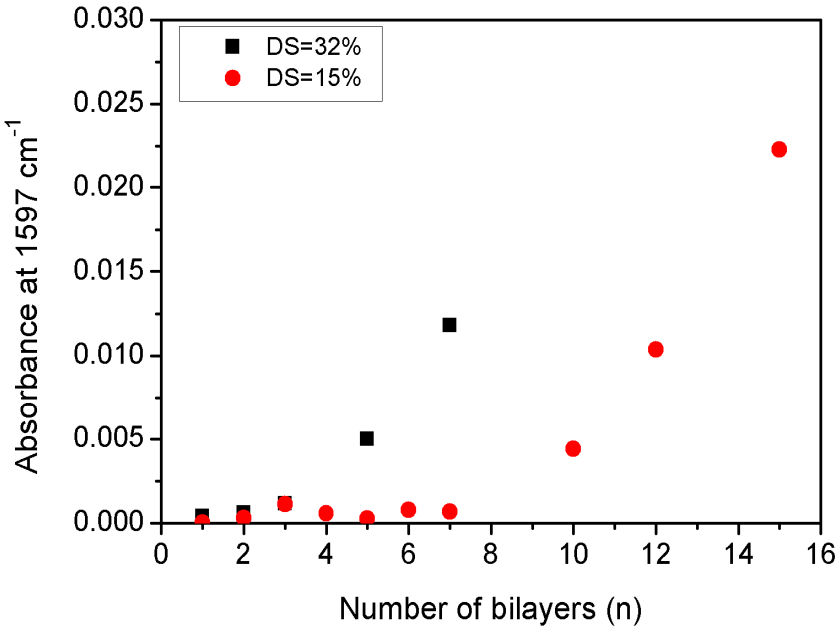

Fig. S5. Evolution of ATR FT-IR absorbance at 1597 cm^{-1} for P4VP as a function of the number of deposited bilayers (n) by using $CHCl_3$ as solvent for P4VP and MEK as solvent for PPFS-MPA-15% and PPFS-MPA-32 %, c = 2 g/L.

(A)

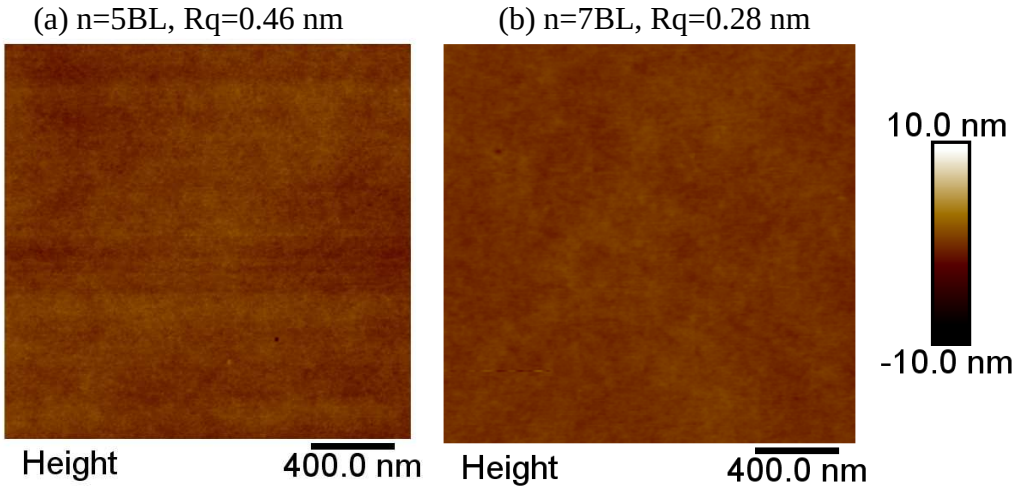

(B)

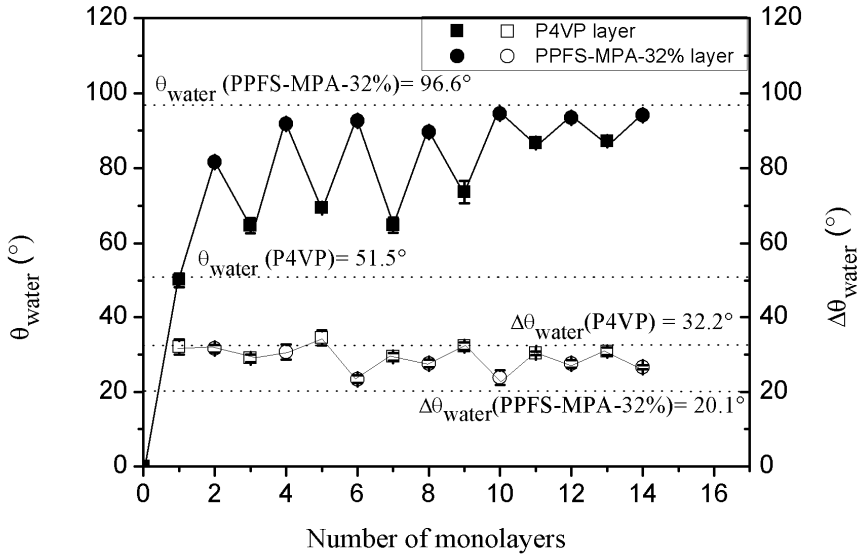

Fig. S6. (A) AFM images collected after a) n = 5 and b) 7 deposited bilayers and (B) θ_{water} (filled symbols) and $\Delta\theta_{water}$ (open symbols) of (P4VP/PPFS-MPA)n ($CHCl_3$ for P4VP and MEK for PPFS-MPA-32%) films measured after each deposited monolayer.

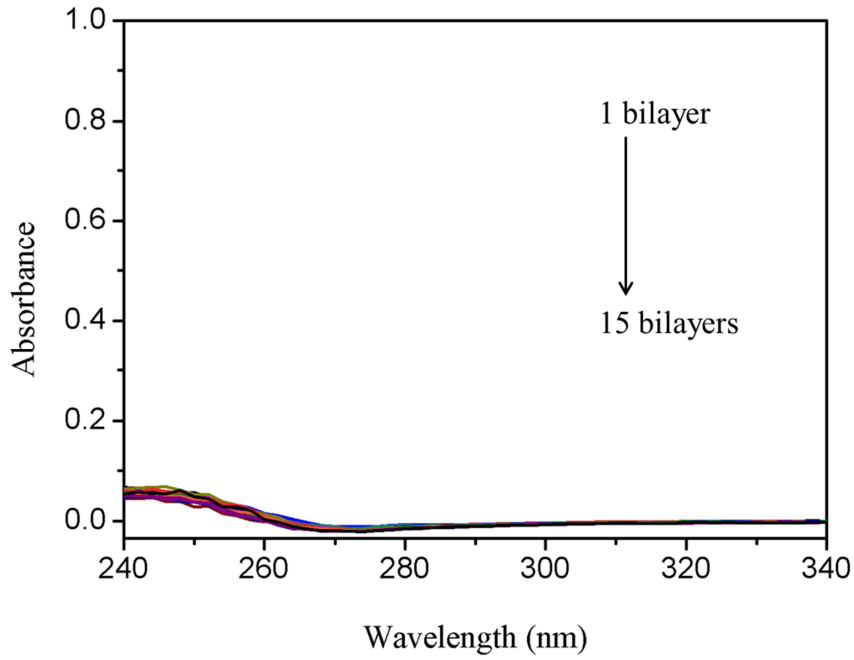

Fig. S7. UV absorbance spectra of (P4VP/PPFS-MPA-32 %)n (DMF) deposited onto glass slide from n=1 to 15 bilayers.

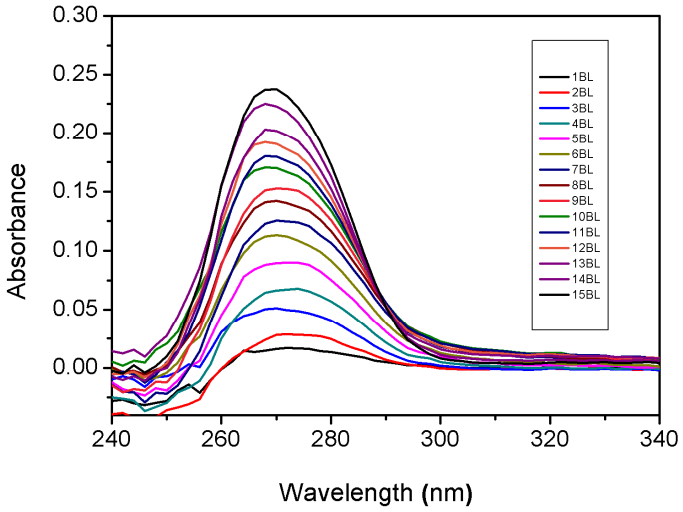

Fig. S8. UV absorbance spectra of (P4VP/PPFS-MPA-32 %)n (Ethanol) deposited onto glass slide from n=1 to 15 bilayers.

Tuning Features of H-bonded Layer by Layer assembly of poly(4-vinyl pyridine) and carboxylated poly-(2,3,4,5,6-pentafluorostyrene) synthesized through para-fluoro-thiol reaction

Quanyi Yin, Emmanuel Beyou, Daniel Portinha, Aurélia Charlot